

THESIS

STREAMFLOW GENERATION ACROSS AN ELEVATION GRADIENT AFTER THE 2020  
CAMERON PEAK FIRE

Submitted by

Quinn Miller

Department of Ecosystem Science and Sustainability

In partial fulfillment of the requirements

For the Degree of Master of Science

Colorado State University

Fort Collins, Colorado

Fall 2022

Master's Committee:

Advisor: Stephanie Kampf

Peter Nelson

John Hammond

Copyright by Quinn Miller 2022

All Rights Reserved

## ABSTRACT

### STREAMFLOW GENERATION ACROSS AN ELEVATION GRADIENT AFTER THE 2020 CAMERON PEAK FIRE

The western United States is experiencing an increase in catastrophic wildfire in virtually all ecoregions. Many of these fires burn in forested headwaters that communities rely on for water supply, underscoring the need for a greater understanding of how wildfire impacts streamflow timing and magnitude. Though many studies have examined the hydrologic response to fire, the site-specific nature of this type of research has made it difficult to generalize findings. The 2020 Cameron Peak fire burned across a broad swathe of the Colorado Front Range, making it an ideal case study to examine the factors that affect post-fire runoff.

The goal of this work is to identify how streamflow responses to rainfall vary from pre-to post-fire conditions and between mountain regions defined by seasonal snow cover and aridity. To this end, we selected three watersheds to compare fire effects on rainfall runoff between snow zones. These watersheds were unburned, moderately burned, and severely burned in each of two snow zones: the high-elevation persistent snow zone, and the mid-elevation intermittent snow zone. These watersheds were instrumented to monitor rainfall and stream discharge throughout water year 2021. To evaluate how wildfire affected runoff, we developed multi-variate statistical models and used Tukey's Honestly Significant Differences test to compare streamflow responses to rainfall between watersheds. Across all burn categories, the high elevation sites were more responsive to rainfall compared to streams at lower elevations; ~50% of rain events produced a streamflow response in the persistent snow zone, compared to ~25% in the intermittent snow

zone. In both snow zones, the unburned sites were the least responsive to summer rainfall and had the highest summer baseflows. Although the high elevation streams were more responsive to rain, they did not exhibit evidence of infiltration excess overland flow. Lags between peak rainfall and peak discharge were 1.2-31.3 hr at these sites; in contrast, the low elevation severely burned site had a much more rapid rise to peak discharge (0.6 hr on average) that indicated infiltration excess overland flow. The rainfall intensity threshold necessary for runoff generation at this site was  $4 \text{ mm hr}^{-1}$ , which agreed with thresholds reported in similar studies of burned areas in this region. We found no evidence that the moderately burned site in the intermittent snow zone generated rapid runoff, likely because that watershed did not experience enough moderate to high burn severity to promote widespread overland flow. Additionally, the flow response at burned sites was uniformly shorter than for the unburned sites in both snow zones. The magnitude of the flow response was higher in the persistent snow zone than in the intermittent snow zone; however, the effect of burn status on streamflow magnitude was difficult to ascertain. These results demonstrate that the streamflow responses to fire vary between snow zones, indicating a need to account for elevation and snow persistence in post-fire risk assessments. Future work in other regions could evaluate whether this snow zone effect is unique to the study area or a common cause of differences in post-fire streamflow.

## ACKNOWLEDGEMENTS

I want to give a big thank you to everyone involved in the development of this research. First and foremost, Stephanie Kampf has been a phenomenal advisor whose expertise, patience, and kindness has been apparent since day one. I couldn't have done this without her guidance and encouragement. Thank you to committee members Peter Nelson and John Hammond for their feedback, and an extra thank you to John Hammond and Marielle Sidell for contributing code that helped in my data analysis. My research has been strengthened by thoughtful suggestions from Megan Sears and Kira Puntenney-Desmond. I am grateful to the lab meetings I had with Clara Mosso, Leonie Kiewiet, David Peterson, Jordyn Geller, Mikaela Richardson, and David Scott. Thank you to Sam Struthers and Cher Prazak for the relentlessly positive attitude they brought to our field monitoring expeditions. I'm thankful to have received funding for this research from the National Science Foundation and the Geological Society of America.

Thank you to the friends and community that supported me personally throughout this process, with an extra thank you to Siwook and Kate for helping out with my fieldwork and generally being wonderful. My parents have always supported and encouraged me, and I am immensely grateful to them for all they do and all they are.

And thank you to Blue the dog, even though he did not help much with the writing.

## TABLE OF CONTENTS

ABSTRACT.....	ii
ACKNOWLEDGEMENTS.....	iv
1. Introduction.....	1
2. Methods.....	5
2.1. Site Description.....	5
2.2. Data Collection and Analysis.....	8
2.3. Drivers of Stream Response to Fire.....	14
3. Results.....	17
3.1. Rain Events and Flow Response.....	17
3.2. Streamflow Response Models.....	32
4. Discussion.....	33
4.1. Differences in Streamflow Generation by Snow Zone.....	33
4.2. Differences in Streamflow Generation by Burn Severity.....	35
4.3. Limitations.....	42
5. Conclusion.....	45
REFERENCES.....	47
APPENDICES.....	53

## 1. INTRODUCTION

Much of the contiguous western U.S. (“the West”) relies on streamflow from mountainous forested watersheds for their freshwater supplies (Brown et al., 2008; Viviroli et al., 2007). In most forested landscapes, nearly all incoming precipitation can infiltrate into the soil and flow through the hillslope as subsurface stormflow (Dunne & Leopold, 1978). This process has the widely recognized benefits of producing clean drinking water and mitigating the effects of flooding (National Research Council, 2008). These regions, however, are experiencing an increase in the size and severity of wildfire due to global climate change (Calder et al., 2015; Westerling, 2016). Though fire is a natural process vital to maintaining ecosystem health in western forests, the changing wildfire regime is likely to impact water quality and availability to western communities (Rocca et al., 2014). As population density increases along the wildland-urban interface in the West, understanding how fire impacts streamflow generation in forested headwaters becomes all the more critical (Hallema et al., 2018).

The current western wildfire regime can be understood by examining past management decisions in addition to the impact of a changing climate (Hallema et al., 2017). As European-American colonization of the West began in earnest in the 1800’s, the genocide of Indigenous peoples and the cessation of the fire stewardship they practiced decoupled the relationship between climate and fire that had existed previously (Higuera et al., 2021). Many western ecosystems that had historically burned frequently saw declining fire activity due to the colonizer’s practice of land use conversion, logging, and active fire suppression (Parks et al., 2015). More than a century of fire exclusion has radically altered the structure of many present-day forests; stands are denser, have lower crown base heights, and are more homogenous with

fewer open patches and meadows (Rocca et al., 2014). These conditions contribute to the effects of 21<sup>st</sup> century warming to increase the likelihood of severe fires occurring (Higuera et al., 2021). Rising temperatures in the West are expected to bring about earlier spring snowmelt, with peak runoff in snowmelt-dominated areas occurring several weeks sooner than in previous decades (Clow, 2010; Fritze et al., 2011; Stewart et al., 2005). This, along with a predicted decrease in summer precipitation and higher fall temperatures, will likely lead to longer wildfire seasons, drier fuel loads, increased area burned, and higher fire severity (Hallema et al., 2017; Rocca et al., 2014; Westerling et al., 2006).

Though many studies have documented how fire disrupts the natural hydrologic cycle at the local or regional scale, the hydrologic response varies across regions differentiated by climate, topography, soil type, and vegetation (Hallema et al., 2016). In most cases, the loss of vegetation leads to more net precipitation reaching the ground (Cawson et al., 2013; Hallema et al., 2017; Kunze & Stednick, 2006). Surface soil sealing and an increase in soil-water repellency are commonly found in post-fire field studies, leading to reduced infiltration. Depending on how soil infiltration has been impacted by the wildfire, incoming precipitation can either permeate through the unsaturated zone or run off as overland flow (Ebel & Moody, 2012). In both cases, post-fire streamflow is increased, though in the latter case much more rapidly and with a greater risk of flooding (Hallema et al., 2017; Moody et al., 2013). In addition to raising peak flows, wildfire can lead to lower baseflows; these effects are typically greatest in the two years following wildfire and fade over time (Saxe et al. 2018). Post-fire runoff response is also heavily influenced by the regrowth of vegetation, which is not always of the same type as what populated the landscape previously (Blount et al., 2020).

Most post-fire assessments in the Colorado Front Range have been conducted for fires at low elevations in semi-arid climates. Though historically this region experienced frequent, low-severity fires, high-severity fires have become more common in the past few decades (Fornwalt et al., 2016; Hallema et al., 2017; Moody et al., 2013). These assessments typically find that high-intensity summer rainfall is likely to trigger destructive floods and mass-wasting events (Benavides-Solorio & MacDonald, 2005). Much less is known about post-fire hazards and their potential triggers in high elevation, high snowpack regions, due to the rarity of severe fires in these areas and the relative inaccessibility of these locations. Subalpine forests in the Front Range have historically experienced high severity fires on time scales ranging from one to multiple centuries, and typically in association with severe drought (Rocca et al., 2014). Though some types of high elevation forests are well-adapted to these kinds of fires (i.e. lodgepole cones opening after fire), predictions of climate change indicate that within 50 years these high elevation, high-severity fires could occur on the scale of decades, rather than centuries (Westerling et al., 2011). There is already evidence that this is happening—fire activity is increasing disproportionately in high-elevation mountain regions, with an upslope advance of ~500 meters in the Front Range (Alizadeh et al., 2021). Additionally, Kampf et al. (2022) found that this region has had a significant increase in the proportion of area burned in the late snow zone, an elevation range they characterize as having a mean annual snow-free date of May 1<sup>st</sup> or later.

To understand the broader implications of the changing fire regime in this region and how it might impact human water use, this study examines the hydrologic response to a high elevation, high-severity fire. The 2020 Cameron Peak fire burned across a large elevation gradient of the Front Range, making it an ideal case study for comparing how post-fire

streamflow generation varies with temperature, aridity, and seasonal snow cover. To that end, this research uses observations from streams located at different elevations and with varying burn severity to quantify the magnitude and timing of streamflow pulses following summer rainstorms. The goal of this work is to examine whether streamflow responses vary from pre-to post-fire conditions and between snow zones and to identify the factors that affect this post-fire runoff.

## 2. METHODS

### 2.1. Site Description

The Front Range, spanning from central Colorado to southern Wyoming, is the meeting point of the easternmost Rocky Mountains and the Great Plains. Elevation in this region ranges from around 1,500 m on the plains to above 4,300 m at the tallest peaks. Vegetation and climate vary greatly along this gradient (Addington et al., 2018). In northern Colorado, the Cache la Poudre River basin covers 2,730 km<sup>2</sup> of the Front Range and supplies water to the cities of Fort Collins and Greeley, as well as numerous agricultural areas. At its highest elevations, the watershed is characterized by dense subalpine spruce-fir forest (*Abies lasiocarpa*, *Picea engelmannii*). At mid-high elevations the landscape transitions to a mixed-conifer forest, composed of mainly lodgepole pine (*Pinus contorta*), Douglas fir (*Pseudotsuga menziesii*), and quaking aspen (*Populus tremuloides*). At its lower elevations, the forest gives way to scattered ponderosa pine stands (*Pinus ponderosa*) and prairie grasses and shrubs. The basin's mean annual precipitation ranges from around 1000 mm in the high elevation headwaters to 330 mm in the grasslands (Richer, 2009).

During the summer months, precipitation in this region comes in the form of high-intensity convective storms that have high spatial and temporal variability (Ebel et al., 2012; Smith et al., 2014). Snow predominates in the winter months. Previous research in this area has identified three distinct patterns of snow cover. The persistent snow zone (PSZ) above ~3,000 m has deep and lasting snow throughout the winter months. The transitional snow zone (TSZ) extends from the lower limit of the PSZ to ~2,600 m and consistently has winter snow, but snow persistence and snow water equivalent is less than in the PSZ. The intermittent snow zone (ISZ)

characterizes the lower elevations where continual snow cover occurs only periodically throughout the winter (Moore et al., 2015; Richer et al., 2013).

By the summer of 2020, bark beetle attacks and drought had left a large portion of the Cache la Poudre watershed's high elevation forest either dead or water stressed (BAER, 2020). The Cameron Peak fire began in these headwaters on August 13, 2020. High temperatures, low humidity, steep terrain, and gusting wind led to extreme fire behavior and rapid spread; by the time it was contained in December it had burned ~845 km<sup>2</sup>, making it the largest fire in Colorado history (BAER, 2020). Post-fire soil burn severity mapping indicates that 20% of the area within the fire perimeter was unburned; 44% was burned at low severity; 30% was moderately burned, and 6% was burned at high severity (Figure 1).

For this study, six catchments were selected in the Cache la Poudre River basin. In the ISZ, one unburned (UI), one moderately burned (MBI), and one severely burned (SBI) site were instrumented; three catchments following the same pattern of burn severity were selected in the PSZ. These are: unburned persistent (UP), moderately burned persistent (MBP), and severely burned persistent (SBP; Figure 1). For the burned study catchments, the USFS Soil Burn Severity map for the Cameron Peak fire (BAER, 2020) was used to determine what percentage of the watershed fell into each burn severity category. The MB sites in each snow zone were burned at moderate and high severity over less than 20% of their area, whereas SBI and SBP had 43% and 45%, respectively, of area burned at moderate and high severity (Table 1). The catchments range in size from 1 to 4 km<sup>2</sup>, are all broadly east-facing, and have slopes ranging from 8 to 33 degrees (Table 2).

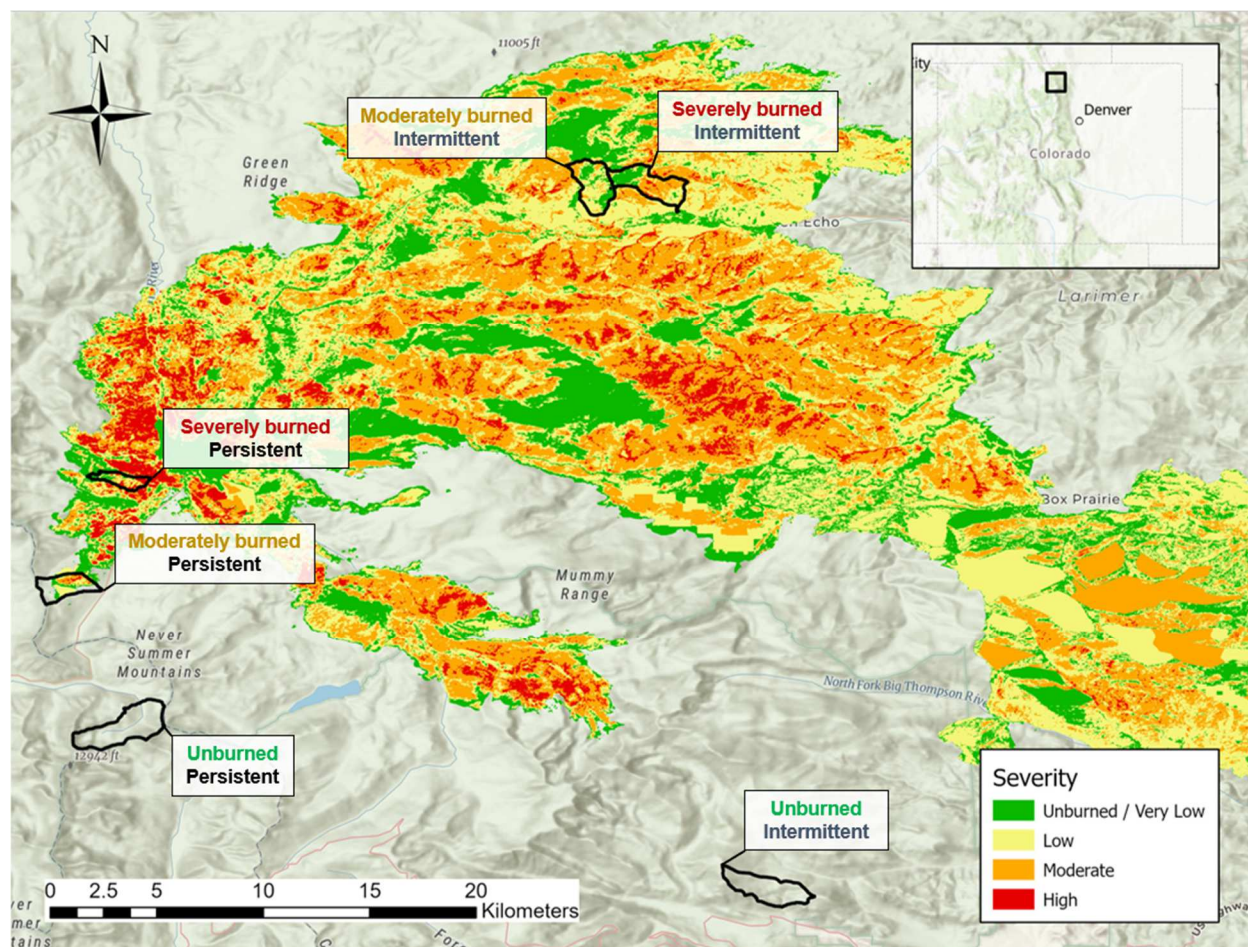


**Figure 1.** Study catchments shown on a soil burn severity map of the Cameron Peak fire (BAER, 2020). The study catchments are characterized by burn severity (unburned, moderately burned, severely burned) and snow zone (persistent or intermittent).

**Table 1.** Percentage of total watershed area in each burn severity category.

Site	Burn Severity (%)			
	Unburned	Low	Moderate	High
MBI	30	55	15	0
SBI	26	31	39	4
MBP	58	25	14	3
SBP	26	30	20	25

**Table 2.** Study catchment characteristics. Site names begin with burn status (unburned, U; moderately burned, MB; severely burned, SB) and end with snow zone (I, intermittent; P, persistent). Characteristics were determined in ESRI ArcGIS Pro using USGS 1m LiDAR DEM for all sites except UI and UP, which were delineated using the USGS StreamStats application (<https://streamstats.usgs.gov/ss/>).

Site	Stream Name	Mean Slope (°)	Aspect	Area (km <sup>2</sup> )	Mean Elevation (m)
UI	Bighorn	19	SE	3.4	2988
MBI	Washout	33	E/SE	2.7	2455
SBI	Dry	18	E/SE	2.5	2753
UP	Michigan	22	N/NE	4.0	3367
MBP	Montgomery	8	E/SE	1.9	3070
SBP	Blue Lake tributary	13	E/NE	1.0	3065

## 2.2. Data Collection and Analysis

The study catchments were instrumented to continuously monitor rainfall and stream stage. Rainfall was monitored using tipping bucket rain gauges attached to data loggers, either an Onset HOBO Pendant event data logger (Onset Computer Corporation, Bourne, MA, USA) or a Campbell Scientific CR1000 data logger (Campbell Scientific Inc., Logan UT, USA; Table 3). A rain gauge was installed near the watershed outlet at each site except for MBI; data from SBI was used for this site because the stream sensors are within 3 km of each other and the watersheds share a drainage divide. Rainstorms were identified using the USDA Rainfall Intensity Summarization Tool, which defined discrete events as being separated by at least 6 hours with less than 1mm of rain (RIST; ARS 2013). For each rain event, RIST calculated depth of precipitation (P; mm); duration of rainstorm (D<sub>p</sub>; hr); maximum intensity (mm hr<sup>-1</sup>) over 5-, 15-, 30-, and 60-minute intervals (MI<sub>5</sub>, MI<sub>15</sub>, MI<sub>30</sub> and MI<sub>60</sub>); kinetic energy (E; MJ ha<sup>-1</sup>); and erosivity (EI<sub>30</sub>; MJ mm ha<sup>-1</sup> hr<sup>-1</sup>).

At most sites, stream stage was continuously monitored using either capacitance rods (TruTrack WT-HR 1000 mm, Auckland, NZ) or pressure transducers (In-Situ Rugged TROLL, Fort Collins, CO, USA; HOBO Water Level Data Logger - U2, Onset Computer Corporation,

Bourne, MA, USA; Table 3). Sites monitored with pressure transducers also had In-Situ Rugged BaroTROLL sensors installed to record and correct for atmospheric pressure. The UP catchment had no flow sensor installed; instead, we used discharge data from the USGS (gage number 06614800; U.S. Geological Survey, 2022), accessed using the “dataRetrieval” package in R (Hirsch et al., 2017). Stream stage at all sites was recorded every 15 minutes except for at SBI, which recorded on 5-minute intervals because the high burn severity in the vicinity of the gage indicated that a dynamic stream response to large rain events was likely.

**Table 3.** The make and model of monitoring equipment used in this study

Site	Rainfall		Stream Water Level	
	Sensor Model	Manufacturer	Sensor Model	Manufacturer
UI	Rainew	Rainwise	Rugged TROLL	In-Situ
MBI	n/a	n/a	U2	HOB0
SBI	TE525	Campbell Scientific	Rugged TROLL	In-Situ
UP	TE525	Campbell Scientific	n/a	n/a
MBP	TE525	Campbell Scientific	WT-HR 1000	TruTrack
SBP	TB3	Hydrological Services	WT-HR 1000	TruTrack

Stream gages were visited monthly from May to October 2021 to download stage data and measure stream discharge. Streamflow was measured using either salt-dilution gaging (Day, 1976) or manually with a velocity meter. During these site visits, stream stage was noted from staff plates affixed to each gage. The change in bed position relative to the gauge bottom was also recorded, as some of the streams in the burn area experienced bed aggradation or incision. These measurements were used to offset-adjust the stage data; for example, if the bed aggraded during an event, the stage record was adjusted up to account for that amount of bed aggradation. Measurements were also adjusted each time the placement of the in-stream sensor changed after a site visit; these instances were easily identified as abrupt steps in stage at the time of data download. These stage data were used to develop stage-discharge rating curves (JMP Pro

Version 15.2.1) and to determine continuous discharge ( $L s^{-1}$ ) at each site (Appendix A). The discharge values were normalized by drainage area to facilitate comparisons and are given in mm/15-min in this study.

To identify runoff from individual storm events, discharge was separated into quickflow and baseflow using a digital baseflow separation filter from the “Ecohydrology” package in R (Fuka et al., 2018). This method of recursive digital filtering by applying a one-parameter signal processing filter comes from Lyne & Hollick (1979). We used 0.98 or 0.99 for the filter parameter value with three passes over the data (Appendix B). This parameter value is higher than what Nathan & McMahon (1990) recommends because lower values did not adequately separate the data (Figure 2). The suggested value was not used because it assigned more of the hydrograph response to baseflow. Although the diurnal stage fluctuations are separated out using the higher filter parameter, these were not assigned as quickflow events. Quickflow events were only assigned to stage rises that exceeded the magnitude of the diurnal fluctuations.

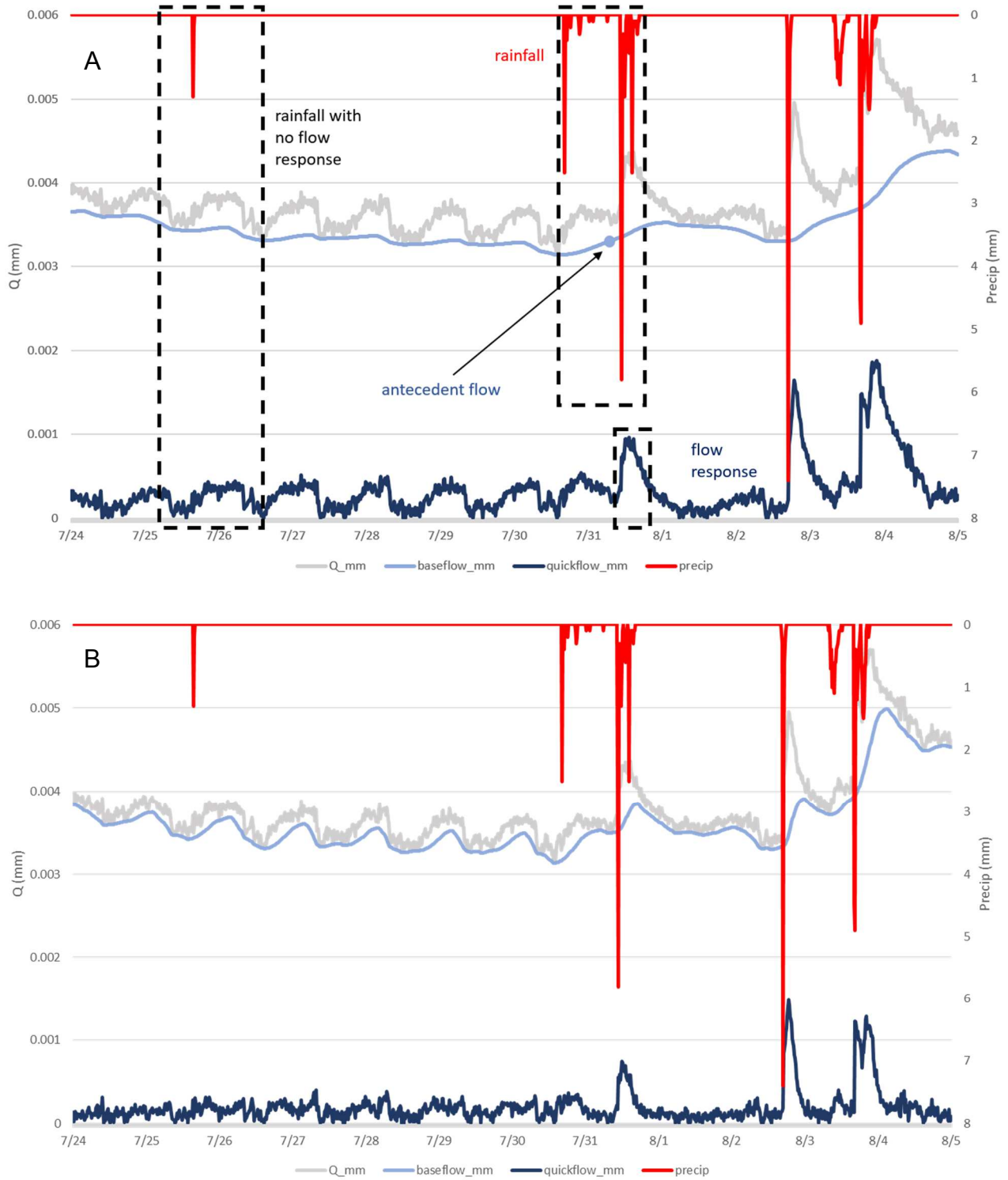


**Figure 2.** Examples of baseflow separation for unburned intermittent (UI) using a filter parameter of 0.98 (A) and the value suggested by Nathan and McMahon (1990), 0.925 (B).

For each site, precipitation and quickflow were plotted together to visually determine if the rainstorm produced a flow response. These quickflow response intervals (QRIs) were defined by Hammond and Kampf (2020) as “subannual periods of discrete quickflow response, in place of the terms event runoff or storm runoff to describe a subannual response to watershed inputs.” To be classified as a QRI, the quickflow data had to be distinct from the background diurnal signal apparent in the filtered data and have occurred within 24 hours of the rain event (Figure 2A). The QRI was determined to start at the first time step with abrupt and distinct hydrograph rise. The QRI end time was more difficult to establish; even after filtering, the quickflow data contained noise and a strong diurnal signal that we did not want to include in our analysis. Additionally, several events were spaced closely enough that the quickflow values did not return to the pre-event baseline before rising again. We thus decided against determining a return to the initial quickflow value as the end of an event. Instead, we defined the QRI end as the time step of the first inflection point of the hydrograph decline following the event peak; this inflection can theoretically be identified where there is a change in the direction of curvature, although in practice it requires some subjective judgment because of noisy data. We interpreted this point as a delineation between the runoff response and the background noise (Barnes, 1939; Figure 3). Rain events that produced a clear stream response were included in further analysis along with those that produced definitively no response. Ambiguous events (those where the stream peak barely rose above background noise levels or occurred asynchronously with the rain event—roughly 20% of events) were not included in further analysis.

Once a QRI was identified, the quickflow data were checked to ensure the filter produced a good baseflow separation. If the quickflow at the first time step of the event was  $\geq 0.0001$  mm, this value of quickflow was assigned as the baseflow quantity because this value corresponds

with incomplete separation of baseflow from quickflow. Next, the following flow metrics were computed: total quantity of quickflow response ( $q_{flow}$ ; mm), magnitude of peak quickflow (peak  $q_{flow}$ ; mm), lag to peak time ( $T_{peak}$ ; hr), duration of response ( $D_{q_{flow}}$ ; hr), time from start of the storm to hydrograph response ( $T_h$ ; hr), duration ratio (DR;  $D_p / D_{q_{flow}}$ ), and runoff ratio (RR;  $q_{flow} / P$ ). Antecedent flow ( $Q_A$ ; mm), a proxy for antecedent soil moisture (Hammond and Kampf, 2020), was determined as the baseflow at the QRI start time (Figure 2).

All rainstorms (the discrete events determined by RIST) identified as producing either a clear response or lack of one were compiled by site. Thresholds for each site were then identified as the  $MI_{60}$  value that maximized the fraction of rain events that correctly predicted a response (Wilson et al., 2018). Cohen’s kappa statistic ( $\kappa$ ) was used to assess the relationship between predicted and observed responses, where values of 0.41-0.60 indicate moderate agreement, 0.61-0.80 indicate substantial agreement, and 0.81-0.99 indicate almost perfect agreement (Viera & Garrett, 2005).

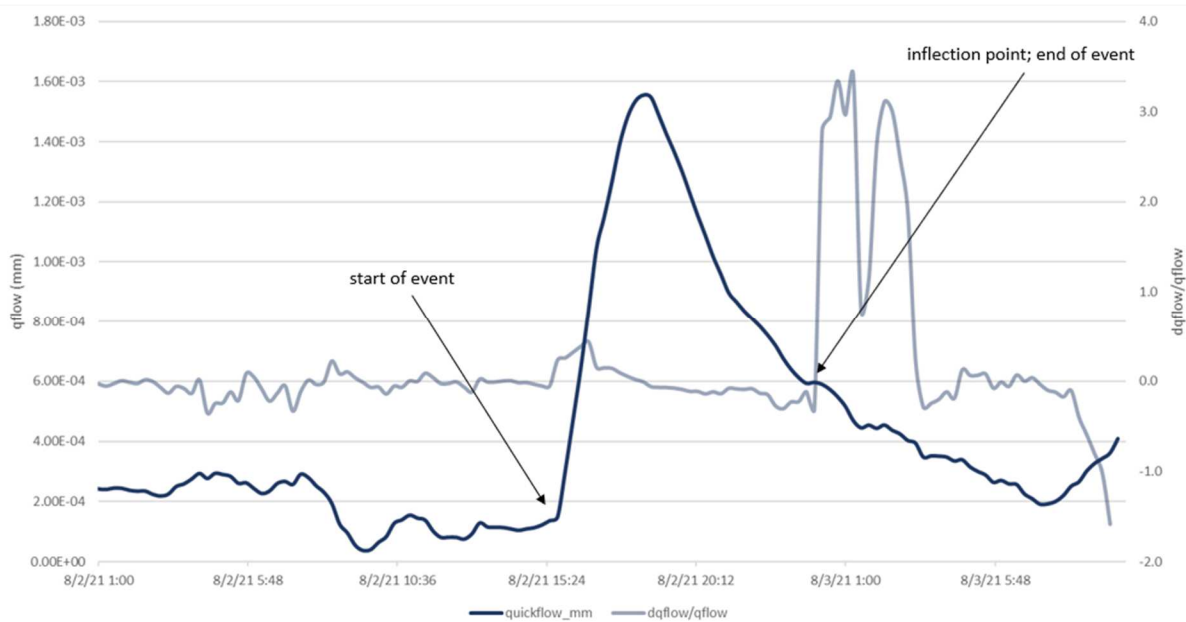


**Figure 3.** Start and end time of the QRI on August 2, 2021 shown in Figure 2. The slope of the quickflow hydrograph, shown on the secondary axis, changes at the inflection point. The data for this figure were smoothed using a moving average filter for better illustration of the methodology.

### 2.3. Drivers of Stream Response to Fire

To evaluate drivers of streamflow responses, we calculated correlations ( $r$ ) between precipitation variables and streamflow metrics and developed multi-variate statistical models. The rain metrics,  $Q_A$ , snow zone (persistent or intermittent), month, and the burn severity categories (unburned, percent burned low, percent burned mid, percent burned high) were considered as potential predictor variables. Month was used to indicate time within the analysis season. These variables were evaluated for collinearity; of variables that were correlated with  $r \geq 0.85$ , only one was chosen to include in the final model (Figure 4A). We decided to include site as a predictor in the model instead of the burn severity and snow zone variables, because site encapsulates the information these variables convey while also allowing for simpler data comparisons. The final selected predictor variables were  $EI_{30}$ ,  $D_p$ ,  $P$ ,  $Q_A$ , month, and site (Table 4).

**Table 4.** The continuous predictor (top) and response variables (bottom) considered for this study. Variables selected for modeling are highlighted in gray.

Variable	Name	Unit or Ratio
P	Precipitation depth	mm
$D_p$	Precipitation duration	hr
MI	Maximum intensity	mm hr <sup>-1</sup>
E	Kinetic energy	MJ ha <sup>-1</sup>
$EI_{30}$	Erosivity	MJ mm ha <sup>-1</sup> hr <sup>-1</sup>
$Q_A$	Antecedent flow	mm
qflow	Quickflow response	mm
peak qflow	Peak quickflow	mm
RR	Runoff ratio	qflow/P
$T_{peak}$	Lag to peak time	hr
$T_h$	Time to hydrograph response	hr
$D_{qflow}$	Duration of response	hr
DR	Duration ratio	$D_p / D_{qflow}$



The same approach of examining collinearity was used to determine which response variables to model (Figure 4B). The qflow and peak qflow variables were highly correlated and both concern the magnitude of flow response, so peak qflow was excluded from modeling. Similarly, both  $T_{\text{peak}}$  and  $T_h$  concern the timing of the flow response; thus, only  $T_{\text{peak}}$  was considered (Table 4). Regression models for each of these stream response metrics were developed using multiple linear regression. After fitting the model, backward selection based on hypothesis testing and a p-value of 0.05 was used to select the final model. Initial graphical checks of the modeling assumptions showed that the data were not normally distributed and had non-constant variance. To address this, both log-based and square-root transformations of the data were considered. Models fit with the log-transformed data better addressed the modeling assumptions, so all response variables were log-transformed and the models re-fit. If a final model included a categorical predictor variable, the estimated marginal mean (EMM) of the response variable was compared across the different levels of the categorical variable using Tukey's Honestly Significant Difference (HSD) test from the "emmeans" package in R (Lenth et al., 2018). Differences in EMM were deemed significant at the  $p = 0.05$  level. Root Mean Squared Error (RMSE) is a metric for evaluating how well a model fits the observed data, with lower values indicating less error. RMSE is influenced by the magnitude of the response variable, so to better facilitate comparisons across models RMSE was normalized by dividing by the interquartile range of observations. These NRMSE values were calculated using the "hydroGOF" package in R along with base R functions (Zambrano-Bigiarini, 2020).

### 3. RESULTS

#### 3.1. Rain Events and Flow Response

The tipping bucket rain gages at each site recorded, on average, 36 individual rain events for each site (Table 5, Figure 5A). The percentage of rain events that produced a response differed between snow zones: the high elevation sites were responsive to 43-57% of events, compared to 19-32% for the low elevation streams. The threshold values of 60-minute rainfall intensity for triggering a response ranged from 0.6-0.9 mm hr<sup>-1</sup> in the PSZ and from 1.4-3.9 mm hr<sup>-1</sup> in the ISZ, further indicating that the high elevation streams were more sensitive to rainfall (Figure 5B). This difference in responsiveness skewed the number of observations for the study catchment clusters: the PSZ had a sample size of 56, more than double the 25 observations from the ISZ. In each elevation grouping, the moderately burned sites were most responsive proportionally and had the lowest thresholds. Agreement between predicted and observed thresholds was high for all sites:  $\kappa$  ranged from 0.7 to 1.0.

**Table 5.** Streamflow response, MI<sub>60</sub> threshold value (T, mm hr<sup>-1</sup>), and corresponding kappa statistic ( $\kappa$ ) for rain events from June to September 2021.

Site	<i>n</i> Rain Events	<i>n</i> Responsive	% Responsive	<i>n</i> Unresponsive	% Unresponsive	T	$\kappa$
UI	43	8	19	28	65	3.8	0.9
MBI	28	9	32	9	32	1.4	0.8
SBI	34	8	24	13	38	3.9	0.8
UP	33	16	49	9	27	0.9	0.8
MBP	37	21	57	12	32	0.6	0.7
SBP	44	19	43	15	34	0.9	1.0

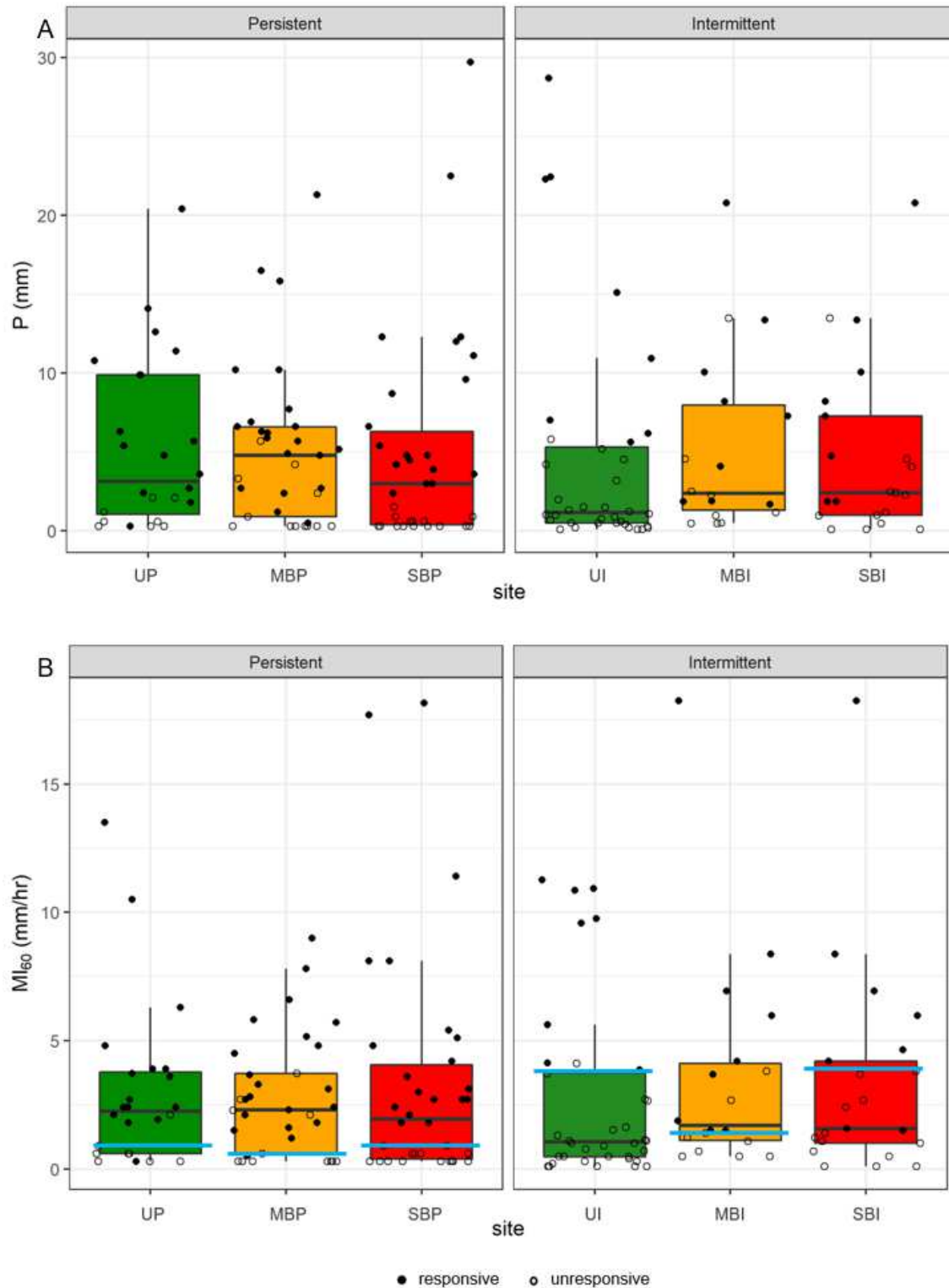


**Figure 5.** Range of (A) P and (B) MI<sub>60</sub> by snow zone and catchment type, with open and closed datapoints representing whether or not that individual rain event had a clear streamflow response. The threshold values of 60-minute rainfall intensity for triggering a streamflow response are indicated by blue lines in (B) and given in Table 5.

General trends in streamflow across snow zone and burn status become apparent when comparing the yearly total discharge ( $Q_{total}$ ), runoff ratio, and full season hydrograph of each study catchment (Table 6; Figure 6). Annual total discharge increased with elevation, from 98-218 mm in the lower catchments to 351-529 mm at the high elevation sites, although most of these sites had incomplete data for calculating annual totals. Similarly, runoff ratio increased with elevation, averaging 0.25 in the ISZ and 0.47 in the PSZ. Antecedent flow ( $Q_A$ ) was overall larger at high elevations—the highest observed  $Q_A$  in the PSZ was 0.03 mm, compared to less than 0.01 mm in the ISZ (Figure 7).

In both snow zones, summer baseflows and  $Q_A$  were lowest for the severely burned streams and highest for the unburned streams. The burned streams also had earlier spring snowmelt and associated hydrograph rise, though this effect was more pronounced in the PSZ. Burn severity did not appear to affect the magnitude of the snowmelt peak in the PSZ. In contrast, UI had a much larger hydrograph peak than the burned intermittent sites, as peak flow was similar for both the moderate and severely burned watersheds.

**Table 6.** Total precipitation ( $P_{total}$ , mm) and discharge ( $Q_{total}$ , mm) for WY2021, and the runoff ratio ( $Q_{total}/P_{total}$ ). Several sites had data missing from this period of record because we installed monitoring equipment at UI, MBP, and SBP in November-December 2020, and at MBI in February 2021. Values for these sites are marked incomplete (i), and the days missing noted. The average runoff ratio ( $Q/P$ ) for 2016-2019 is available from previous research for UI, SBI, and UP.  $P_{total}$  was obtained from gridded PRISM data (PRISM Climate Group, 2004) because tipping bucket rain gages do not accurately capture winter precipitation.

Site	$P_{total}$ (mm)	$Q_{total}$ (mm)	$Q_{total}/P_{total}$	$Q/P^1$	Days Missing
UI	696	218 <sup>i</sup>	0.31 <sup>i</sup>	0.04	79
MBI	444	98 <sup>i</sup>	0.22 <sup>i</sup>		156
SBI	437	132	0.30	0.14	
UP	1045	476	0.46	0.64	
MBP	996	529 <sup>i</sup>	0.53 <sup>i</sup>		49
SBP	815	351 <sup>i</sup>	0.43 <sup>i</sup>		46

<sup>1</sup>Average runoff ratio for 2016-2019 from Harrison et al. (2021).

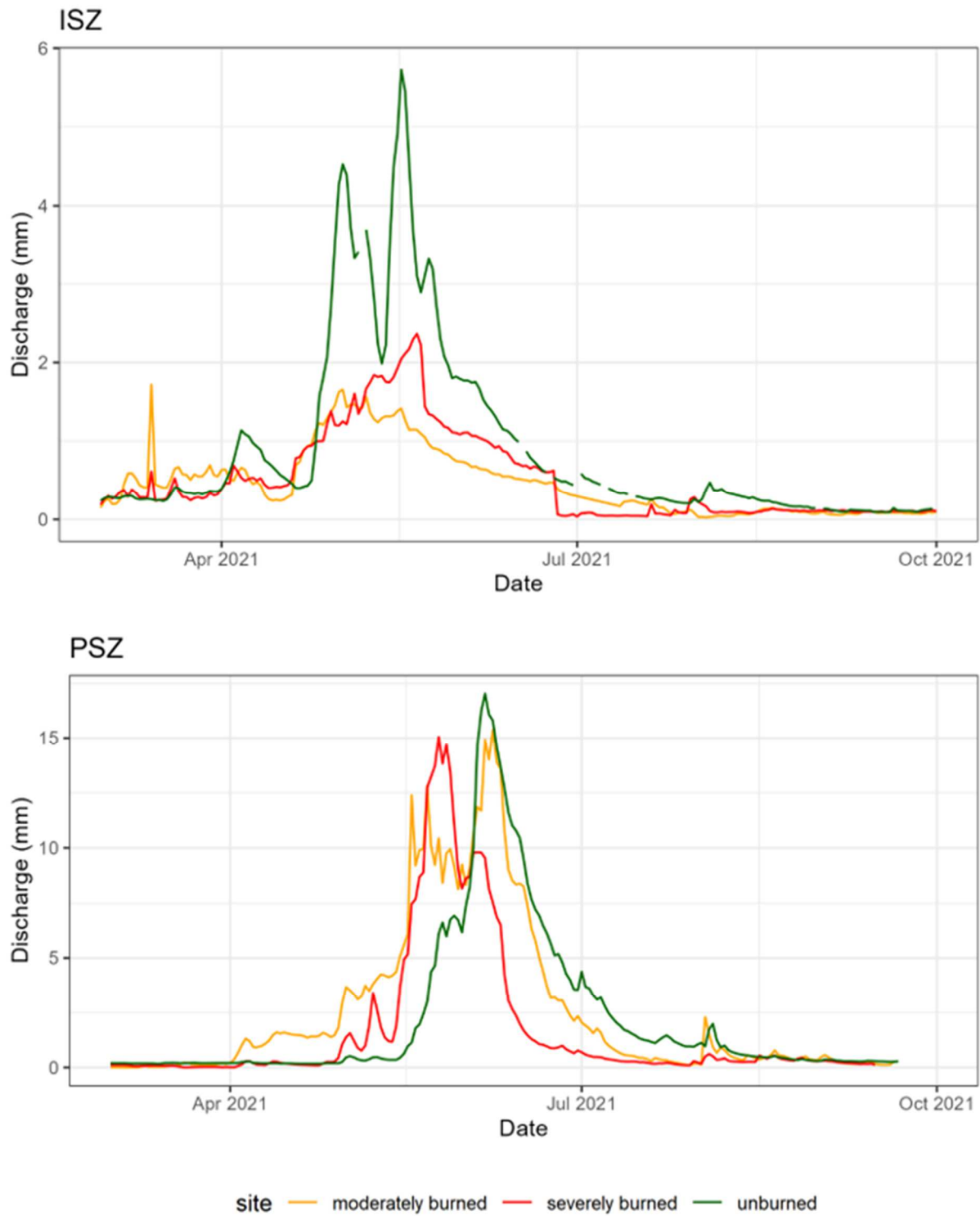


**Figure 6.** Water year 2021 hydrographs for all sites by snow zone and catchment type, showing daily time steps.

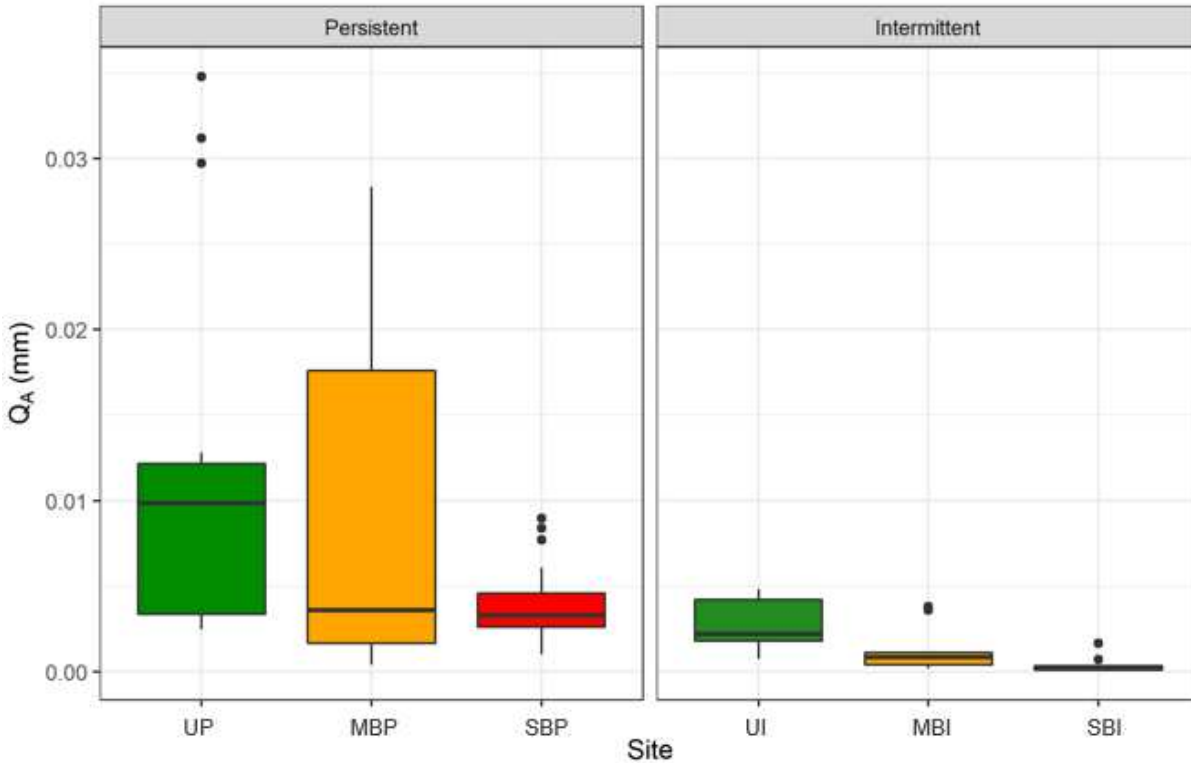


**Figure 7.** Range of antecedent flow ( $Q_A$ ) by snow zone and catchment type.

In both the PSZ and the ISZ, the total quantity of the quickflow response (qflow) was lowest in the severely burned catchments; the average qflow values for SBI and SBP were 0.04 mm and 0.10 mm, respectively. However, the ranges of qflow overlapped for all burn categories in each snow zone (Figure 8A). The qflow values were an order of magnitude higher in the PSZ compared to the ISZ; the highest qflow was 0.20 mm in the ISZ and 2.1 mm in the PSZ. Runoff ratio (RR) followed a similar pattern of the severely burned sites having the lowest values. Unlike qflow, however, the highest average values for RR were at the moderately burned sites in both snow zones; RR was 0.01 at MBI and 0.05 at MBP (Figure 8B).

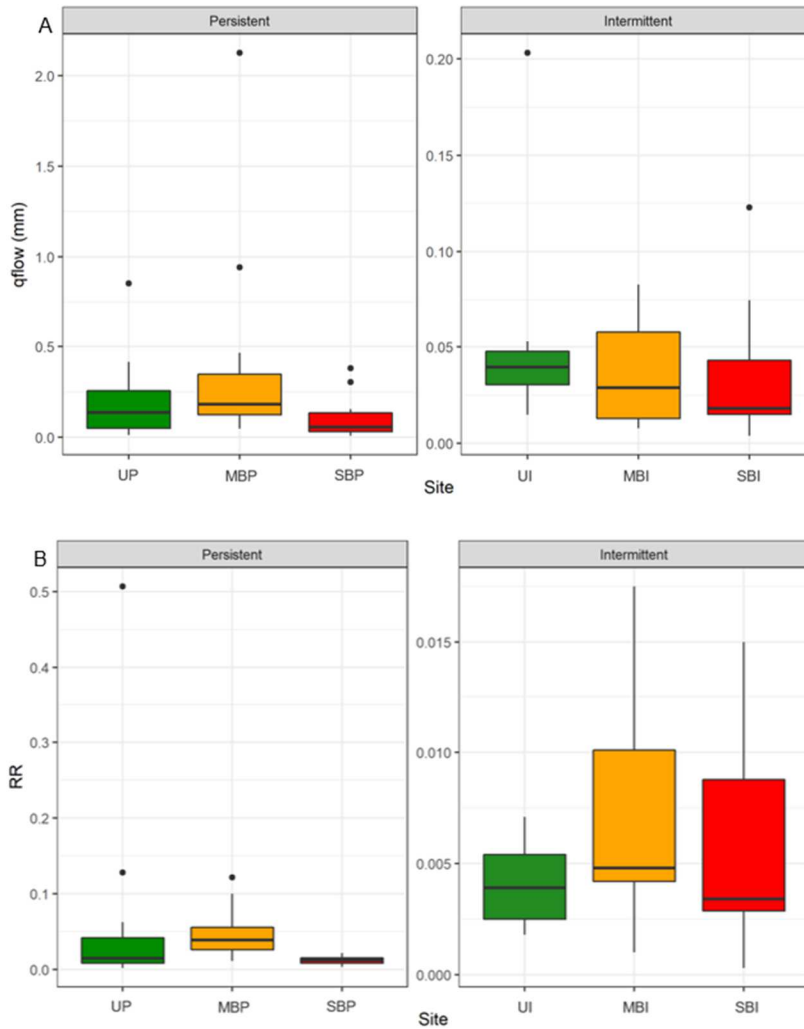


**Figure 8.** Range of (A) total quantity of quickflow response (qflow), (B) runoff ratio (RR), (C) lag to peak time ( $T_{peak}$ ), (D) duration of response ( $D_{qflow}$ ), and (E) duration ratio (DR) by snow zone and catchment type. To better illustrate the spread of the data, the y-axis is scaled differently for the ISZ and PSZ plots and the RR values for persistent sites in (B) are displayed on a log scale.

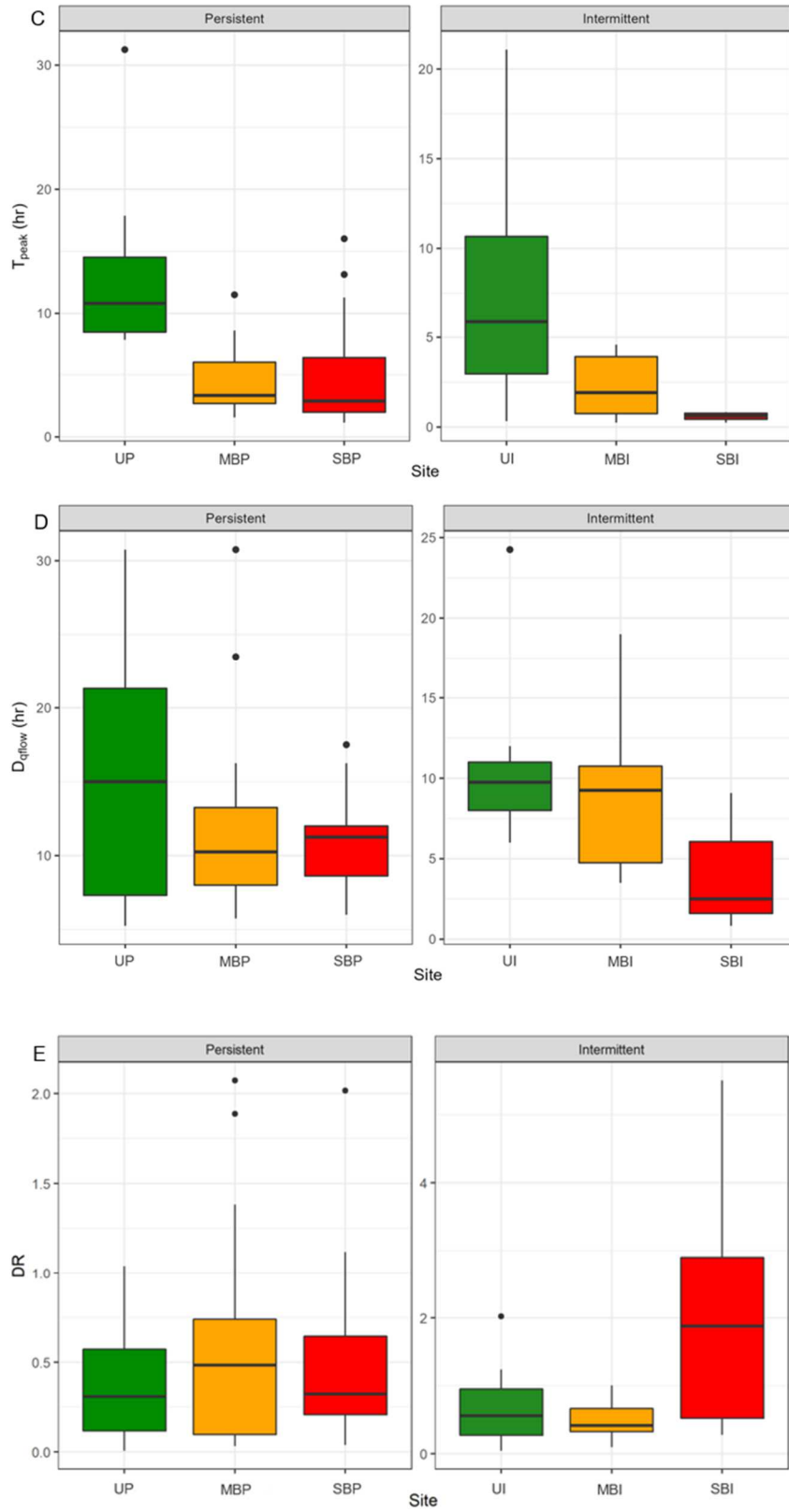
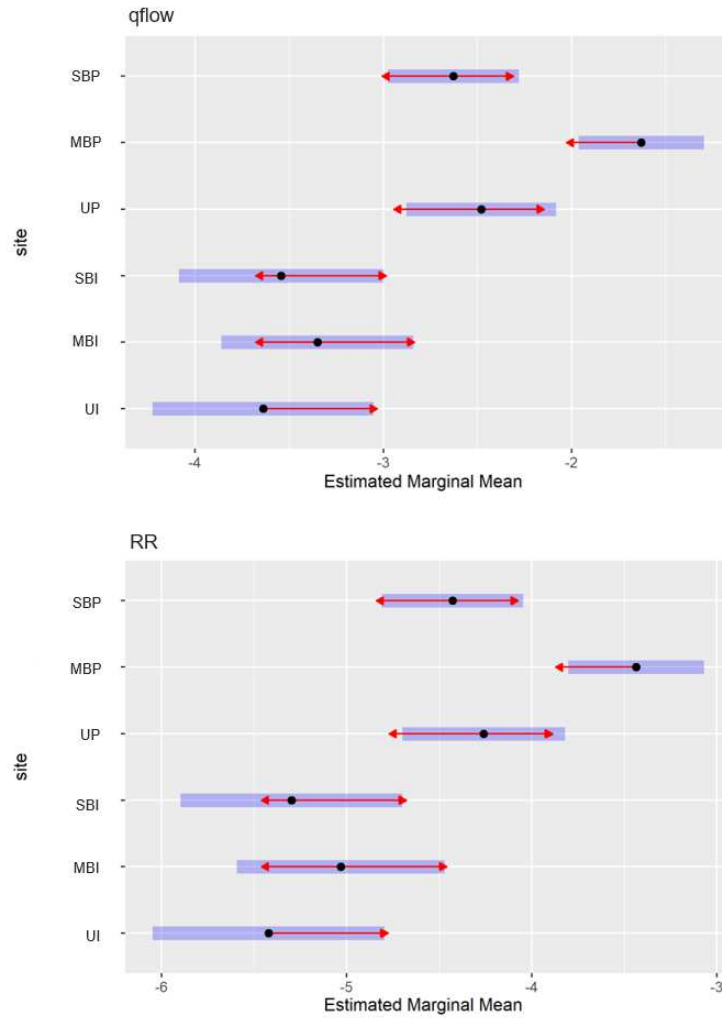


Figure 8, continued.

Considering the streamflow response variables related to timing, the lag to peak time ( $T_{\text{peak}}$ ) and duration of response ( $D_{\text{qflow}}$ ) were both generally lowest at the severely burned sites and lower in the ISZ compared to the PSZ. The average  $T_{\text{peak}}$  values at SBI and SBP were 0.58 hr and 4.93 hr, respectively, and the average  $D_{\text{qflow}}$  values at SBI and SBP were 3.82 hr and 10.76 hr, respectively. The unburned sites had the longest lags to peak; on average 7.8 hr at UI and 12.6 hr at UP (Figure 8C). The average  $D_{\text{qflow}}$  at UI and UP was 11.14 and 15.66 hr, respectively (Figure 8D). In contrast, the relationship between burn severity and duration ratio (DR) is less apparent. All sites except SBI had similar values for DR, ranging from  $\sim 0.1$ -  $\sim 0.8$ . The average DR at SBI, however, was 2.16 (Figure 8E).  $T_{\text{peak}}$  value ranges overlapped between snow zones, with higher values possible in the PSZ.  $T_{\text{peak}}$  ranged from 0.25-21.08 hr in the ISZ and from 1.15-31.25 hr in the PSZ.  $D_{\text{qflow}}$  values for sites in the PSZ were generally larger than their counterpart in the ISZ ( $D_{\text{qflow}}$  ranged from 0.83-24.25 hr in the ISZ and from 5.25-30.75 hr in the PSZ), though not by the same order of magnitude as seen in the streamflow quantity variables discussed above.

The multivariate modeling of streamflow variables enabled statistical comparisons of these variables between sites. Comparisons for the qflow and RR models identified a significant difference between MBP and all other sites, and between UI and UP. In the  $T_{\text{peak}}$ ,  $D_{\text{qflow}}$ , and DR models, the EMM for SBI was different from the other sites; the  $T_{\text{peak}}$  model identified UP as being significantly different from all other sites as well (Figure 9).



**Figure 9.** Tukey-adjusted pairwise comparisons of log-transformed response variables by site. The blue bars are confidence intervals for the estimated marginal mean (EMM), and the red arrows indicate comparisons. If an arrow from one site's EMM overlaps another, then the difference between the two sites is not significant at the  $p=0.05$  level.

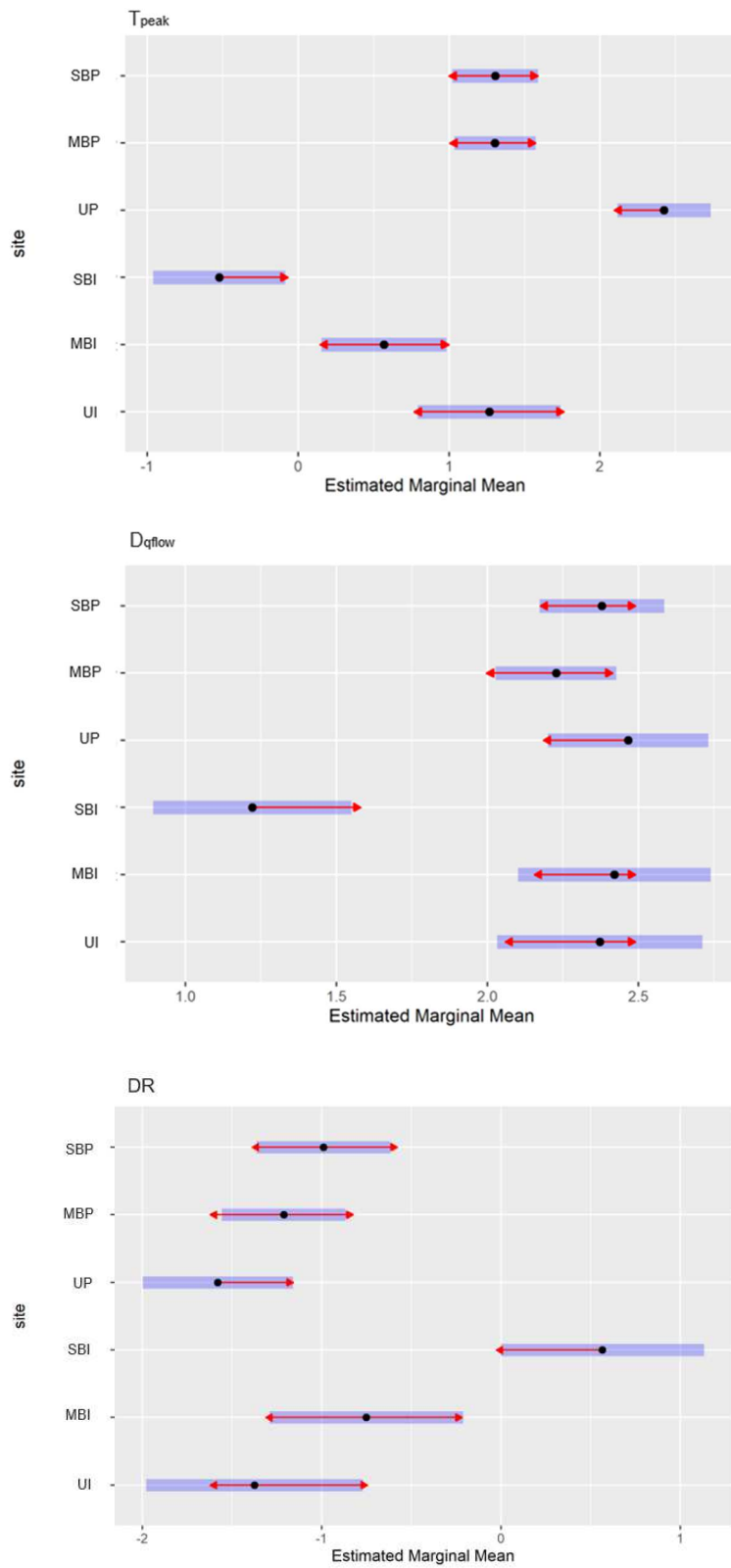
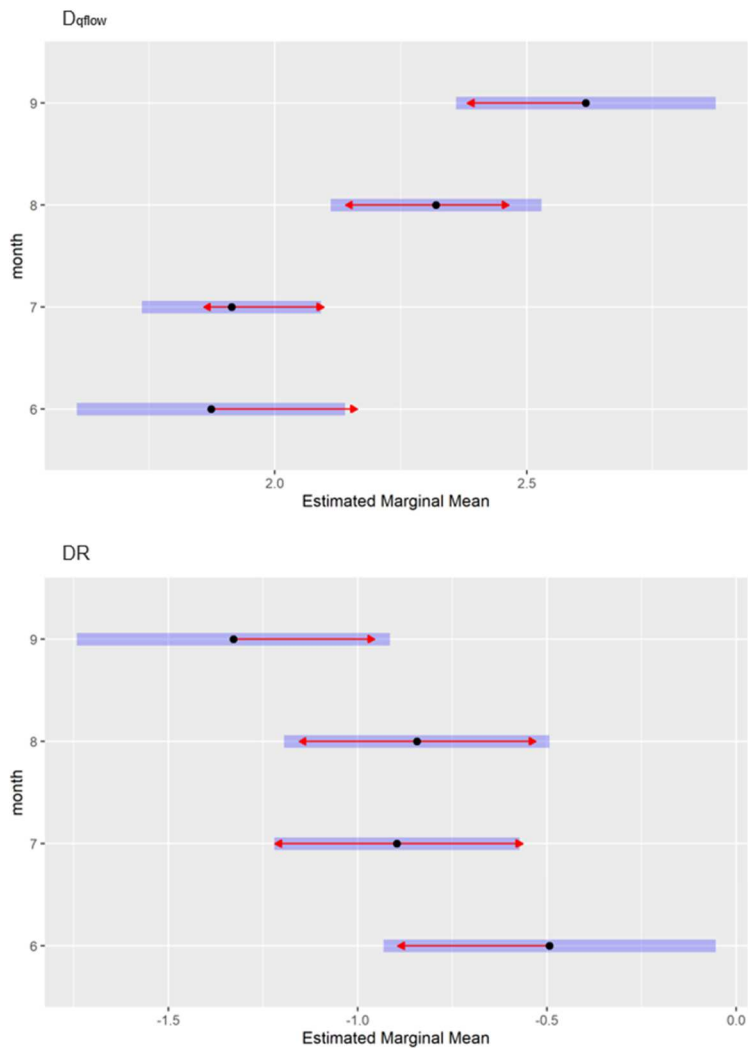


Figure 9, continued.

The final models for  $D_{qflow}$  and DR included month as well as site as categorical predictors. Figure 10 shows a clear trend towards longer  $D_{qflow}$  and shorter DR from June to September, meaning the response durations increased through the season. The average  $D_{qflow}$  was 8.90 hr in June and 15.10 hr in September. The average DR was 1.05 in June and 0.52 in September. The p-values for all Tukey HSD comparisons of site and month can be found in Appendix C.



**Figure 10.** Tukey-adjusted pairwise comparisons of  $\log(D_{qflow})$  and  $\log(DR)$  by month. The numbers 6-9 indicate the months June-September.

Univariate correlations help illustrate how the rainfall metrics relate to streamflow response variables. The response variables were each significantly correlated with at least one rainfall variable (Figure 11). Of the response variables concerning the magnitude of the flow response, qflow was significantly correlated with P ( $r = 0.41$ ), and RR was significantly correlated with  $Q_A$  ( $r = 0.52$ ). Concerning the timing variables,  $T_{peak}$ ,  $D_{qflow}$ , and DR were all correlated with  $D_p$  ( $r = 0.61$ ,  $0.46$ , and  $0.41$ , respectively). These correlations had a higher p-value than the correlations between those same response variables and P.



**Figure 11.** Correlation matrix between streamflow response variables and rainfall and antecedent condition variables. With 80 observations, Pearson’s for critical values at  $p = 0.05$  is 0.217—significant correlations that exceed this critical value are in bold.

The correlation coefficients in Figure 11 grouped all sites together; distinct patterns were evident between the individual sites in Figures 12 and 13. For example, the total precipitation (P) was more correlated to quickflow (qflow) in the PSZ compared to the ISZ sites: the correlation coefficients for the high elevation streams ranged from 0.59-0.97, compared to 0.07-0.79 for the

intermittent sites. Antecedent flow ( $Q_A$ ) was also positively correlated with RR at most sites, with a clear distinction between the unburned and severely burned streams in both snow zones. The correlation coefficient for UP was 0.84, compared to 0.26 at SBP; similarly, UI had a coefficient of 0.12, compared to -0.41 at SBI.

For streamflow timing variables, the precipitation duration ( $D_p$ ) was positively correlated with lag to peak ( $T_{peak}$ ) in both the PSZ and the ISZ. The strongest correlations were in the unburned catchments in both snow zones; the coefficients for UI and UP were 0.98 and 0.93, respectively.  $D_p$  and the duration of response ( $D_{qflow}$ ) were more highly correlated in the PSZ (average  $r$ : 0.45) than in the ISZ (average  $r$ : 0.26), with the severely burned sites in each snow zone having the lowest correlation (0.18 for SBP and -0.17 for SBI). The relationship between  $D_p$  and duration ratio (DR) is not included graphically here because  $DR = \frac{D_p}{D_{qflow}}$ ; therefore, all sites showed a strong positive correlation between the two variables.

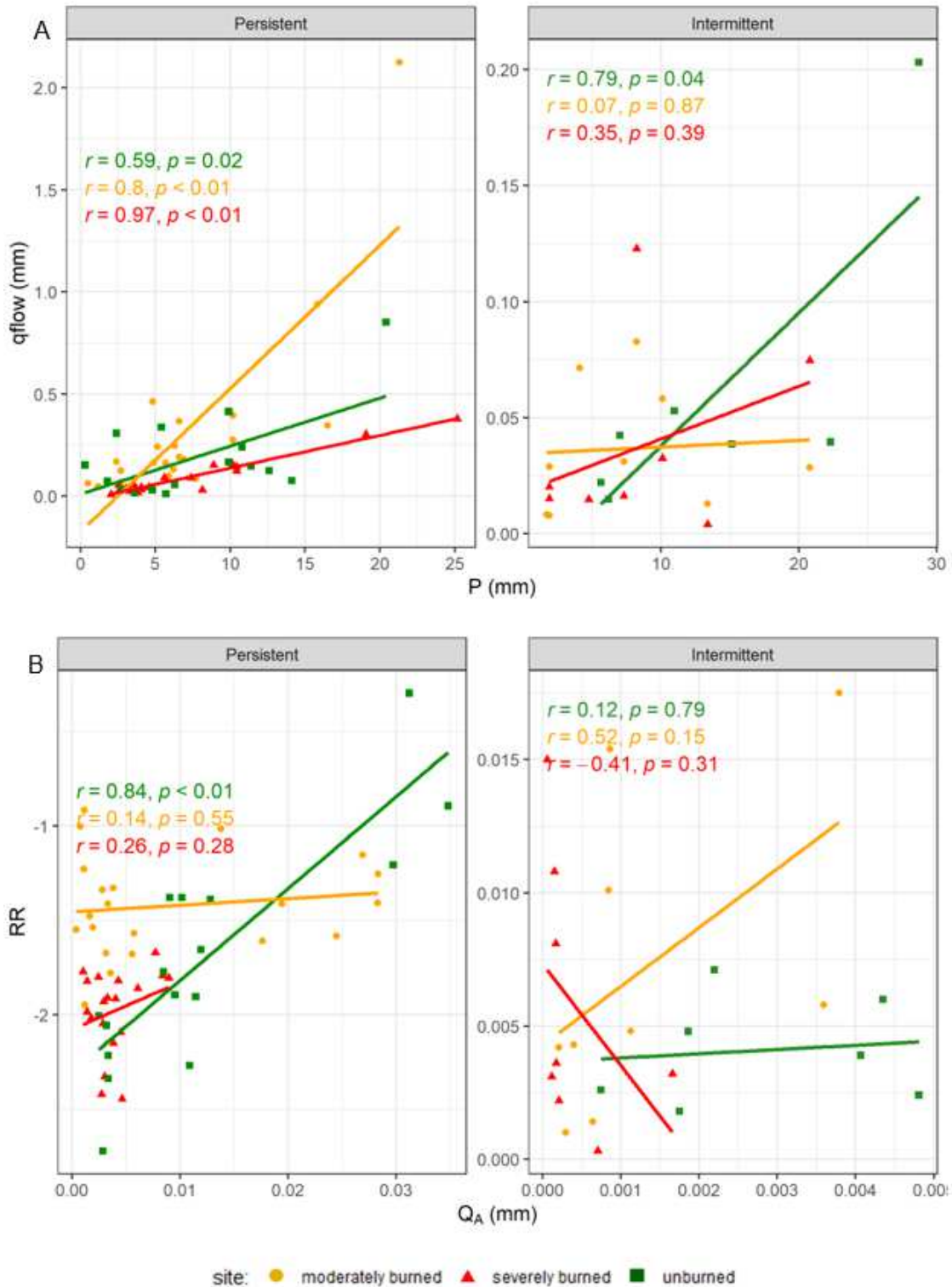


**Figure 12.** Scatterplots showing (A) P vs. qflow and (B)  $Q_A$  vs. RR by snow zone and catchment type. To better illustrate the spread of the data, the y-axis is scaled differently for the ISZ and PSZ plots and the RR values for persistent sites in (B) are displayed on a log scale. Correlation coefficient and the corresponding p-value for individual sites are shown in each plot.

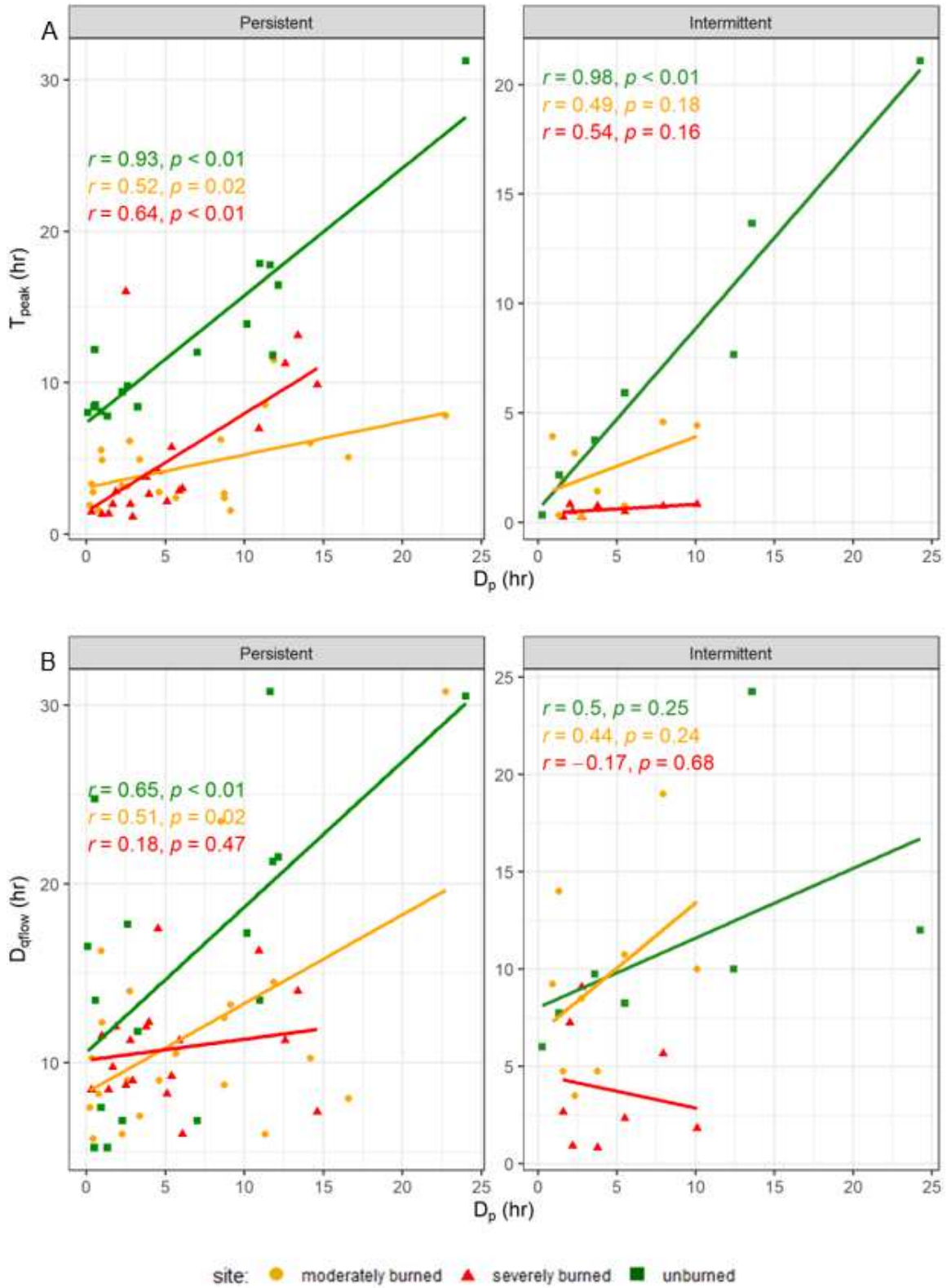


**Figure 13.** Scatterplots showing (A)  $D_p$  vs.  $T_{peak}$  and (B)  $D_p$  vs.  $D_{qflow}$  by snow zone and catchment type. To better illustrate the spread of the data, the y-axis is scaled differently for the ISZ and PSZ plots. Correlation coefficient and the corresponding p-value for individual sites are shown in each plot.

### 3.2. Streamflow Response Models

Multivariate models of streamflow response variables performed reasonably well. The  $T_{\text{peak}}$  ( $R^2 = 0.73$ ) and  $q_{\text{flow}}$  ( $R^2 = 0.67$ ) models had the best fit and the lowest NRMSE values. The RR model performed the worst ( $R^2 = 0.59$ ), and the  $D_{q_{\text{flow}}}$  and DR models had the highest NRMSE. For the streamflow magnitude variables, predictors identified for  $q_{\text{flow}}$  and RR were  $Q_A$  and site; the  $q_{\text{flow}}$  model also included P. For streamflow timing variables, the models for  $T_{\text{peak}}$ ,  $D_{q_{\text{flow}}}$ , and DR all had  $D_p$  and site as predictors. Additionally, the two models concerning the duration of the flow response ( $D_{q_{\text{flow}}}$  and DR) both included month, but only DR included  $Q_A$  as a predictor as well. Though  $EI_{30}$  was considered as a predictor for each model, it was not selected for any. Overall,  $Q_A$  appeared to be the most reliable predictor for the streamflow magnitude variables, and  $D_p$  for the streamflow timing variables. The coefficients for all the streamflow response regression models are shown in Table 7.

**Table 7.** Coefficients ( $\beta$ ) for multiple linear regression models of each streamflow response variable ( $y$ ), with performance indicated by multiple  $R^2$  and NRMSE. The variables are defined in Table 4. Cells are left blank when a variable is not included in the model. A “+” indicates that a categorical variable was used in the model, and these coefficients can be found in Appendix D.

$y$	$\beta_0$	$\beta_1 P$	$\beta_2 D_p$	$B_4 Q_A$	Month	Site	$R^2$	NRMSE
<b>qflow</b>	-4.82	0.11		46.11		+	0.67	0.42
<b>RR</b>	-5.76			54.22		+	0.59	0.43
<b><math>T_{\text{peak}}</math></b>	0.79		0.08			+	0.73	0.40
<b><math>D_{q_{\text{flow}}}</math></b>	1.77		0.03	21.41	+	+	0.63	0.65
<b>DR</b>	-1.92		0.16		+	+	0.66	0.48

## 4. DISCUSSION

This study compares three catchments, ranging from unburned to severely burned, in each the intermittent snow zone and the persistent snow zone of the Cache la Poudre River basin. Through examination of differences in streamflow magnitude and timing following summer rainstorms, this study provides insights into how both snow zone and wildfire affect rainfall runoff.

### 4.1. Differences in Streamflow Generation by Snow Zone

Colorado is known as a headwater state, and the images of snow-capped peaks that adorn everything from tourism brochures to the state license plate reflect the connection between snowy mountainous areas and the state's most important resource. Indeed, studies have found that 74% of runoff in the Front Range originates from seasonal snowpack (Li et al., 2017). Of the areas that receive seasonal snow, high elevation catchments with deep winter snow have been found to contribute more flow per unit area than those in areas of patchy snow cover (Hammond et al., 2018; Harrison et al., 2021). Previous research in the Cache la Poudre River basin has described an abrupt shift in hydrologic regime between the PSZ and the ISZ; discharge and runoff ratios were orders of magnitude higher at high elevation catchments compared to intermittent snow catchments (Harrison et al., 2021). While these previous studies focused more on total water yield, the current study examines the details of rainfall-runoff events. The findings demonstrate that the increase in discharge with elevation is also present for rainfall runoff in both burned and unburned conditions.

We considered streamflow response to individual summer rain events and found that the total quantity of quickflow response and runoff ratios were consistently higher in the PSZ than in

the ISZ. These responses were small compared to the hydrograph peaks due to snowmelt runoff—rainfall runoff efficiency is generally lower than snowmelt-induced flow because soil moisture decreases during the summer months (Figures 6 and 8). There are also differences in soil moisture content between snow zones. Harrison et al. (2021) found that volumetric water content (VWC) in the persistent snow region of the Cache le Poudre River basin ranged from 0.2-0.6 between 2016-2019, compared to 0.1-0.2 for intermittent sites. Similarly, antecedent flow was higher at the PSZ sites considered in this study than at the ISZ sites (Figure 7). The positive correlation we found between RR and  $Q_A$  at high elevations (Figure 12), and the inclusion of  $Q_A$  in both streamflow magnitude (qflow and RR) models indicate that higher antecedent soil moisture content increases the likelihood that incoming precipitation will cause a streamflow response. These results agree with another study of streamflow generation in semiarid climates; wet antecedent conditions were shown to be correlated with significantly higher runoff in an unburned catchment in New Mexico (Schoener & Stone, 2019). Other studies have shown that wetter hillslope conditions are correlated with the expansion of macropore systems, allowing larger volumes of water to move through the subsurface in the same amount of time (Sidle et al., 1995).

One driver of the higher streamflow at high elevations is precipitation. The qflow model included precipitation as a predictor, which is consistent with previous research that found that flow volume is highly controlled by P in watersheds throughout the West (Hammond et al., 2018). The correlation between P and qflow is strongest in the PSZ, with the same increase in P associated with a much smaller increase in qflow in the ISZ (Figure 12A).

In the ISZ, winter temperatures periodically rise enough to induce mid-season melt, resulting in an overall shallow snowpack. Come spring, snowmelt at this elevation is usually

insufficient to saturate near-surface soils and recharge groundwater (Harrison et al., 2021). Accordingly, incoming summer precipitation would go to recharging long term groundwater storage and produce no observable stream response (for unburned conditions; the observed effect of fire on infiltration is discussed in section 4.2.). We observed that rain events with a  $MI_{60}$  of 1.4-3.9  $\text{mm hr}^{-1}$  were necessary to trigger a quickflow response; conversely, rainstorms with  $MI_{60} \leq 0.90 \text{ mm hr}^{-1}$  could have a flow response in the PSZ. The magnitude of the responses in the ISZ were usually quite small in comparison to the magnitude of responses in the PSZ (Figure 6).

#### **4.2. Differences in Streamflow Generation by Burn Severity**

The burned ISZ sites had generally higher quickflow magnitudes than their unburned counterpart, though the average values at these burned sites were lower. In contrast, the magnitude of the flow response overlapped for burned and unburned PSZ sites, indicating an ambiguous relationship between wildfire and the magnitude of the streamflow response to rain. The effect of wildfire on the magnitude of summer baseflows was clearer; the severely burned sites had the lowest baseflows, and the unburned sites the highest (Figure 6). Decreased baseflow following wildfire and other forest disturbances is documented in the literature; it is usually associated with changes in snowmelt timing and magnitude and the regrowth of vegetation (Goeking & Tarboton, 2020; Harpold et al., 2015 Perry & Jones, 2017). Earlier melt and reduced infiltration of meltwater impacts patterns of soil moisture through the summer months, leading to lower baseflows.

The ambiguity we observed between wildfire and quickflow magnitude may be because site was consistently significant as a predictor variable in the multiple linear regression models, which indicates that site-specific characteristics had a large influence on the magnitude and

timing of the flow response. These influences could be burn pattern and snow zone, which we intended for site as a variable to encompass, but they could also be characteristics such as network morphology and connectivity, soil type and depth, or other features not accounted for in this study. These confounding factors may obscure patterns between burn severity and some of the streamflow response variables. For example, qflow and RR showed no clear relation to burn status other than the severely burned sites uniformly had the lowest RR (Figure 8). Post-fire streamflow is extremely variable and peak flows have been observed to decrease following a disturbance; however, most previous studies specific to this region have found that water yields increased following wildfire—in some cases by more than 200% (Blount et al., 2020; Goeking & Tarboton, 2020; Hallema et al., 2017; Moody & Martin, 2001). Increased flow is also expected following widespread tree mortality because low vegetation density decreases evapotranspiration and increases the hydrologic connectivity of the subsurface (Emanuel et al., 2014). Although post-fire vegetation was not quantified here, field visits to SBI and SBP gave the impression of almost total tree mortality with little regrowth occurring throughout the monitoring period. For these reasons, the relatively low streamflow at the severely burned sites may not be indicative of the effects of fire. One explanation for the low discharge and runoff observed at burned sites could be that they are net losing streams, acting to recharge groundwater. In mountainous areas, regional groundwater flow between basins is controlled by large, well-incised drainage network (Gleeson & Manning, 2008). SBP, MBI, and SBI are all small, first-order headwater streams without much channel incision, and thus could be perched too high to gain flow from the groundwater that runs through deeper subsurface flowpaths.

One burned site—MBP—had higher values of qflow and RR than its corresponding unburned catchment. It is unlikely that these high values are solely a burn effect—only 3% of

MBP burned at high severity compared to 25% of SBP, yet the highest qflows at MBP were more than double those at SBP. Furthermore, the annual runoff ratio for MBP was 0.53, compared to 0.43 at SBP (Table 6). Instead, the high values of discharge and runoff ratio observed at MBP could be due to its local topography. The sensor at MBP was installed in a flat valley bottom (the watershed had the lowest average slope of 8%), where flow paths converge. In contrast, the gages in other burned watersheds were located along steeper channel stretches, in watersheds with higher average slope. Locally flat areas in otherwise steep subalpine regions can have longer snow persistence and wetter average soils that allow saturation overland flow to develop (Kampf et al., 2015). MBP had some of the highest recorded values of  $Q_A$ , and observations made during field visits to this site noted numerous large swales in the vicinity of the stream gage that remained saturated and marshy through most of the monitoring period.

Unlike the streamflow magnitude response variables, burn effect was more evident for the variables concerning the timing of the flow response. All the burned watersheds had lower lag to peak times and shorter response durations than their unburned counterparts, suggesting that runoff in these catchments was produced through infiltration excess overland flow for at least some of the summer rainstorms. SBI may be the only site that experienced consistent and widespread overland flow; Tukey HSD comparisons between sites identified SBI as having significantly shorter  $T_{peak}$  and  $D_{qflow}$  than the other sites. Additionally, the duration of the rain event was the most consistently significant predictor for the streamflow timing variable:  $T_{peak}$  and  $D_{qflow}$  were strongly positively correlated with  $D_p$  for all sites except SBI. That the timing of the flow response at SBI was not much influenced by the length of the precipitation input is also evidenced by its duration ratio ( $D_p/D_{qflow}$ ), which was significantly higher than all others.

MBI and SBI are similar catchments in terms of climate, geology, geomorphology, and ecology, yet the hydrograph at MBI does not indicate that infiltration excess overland flow occurred there at the same scale as it did at SBI. In addition to the differences in magnitude of  $T_{\text{peak}}$  and  $D_{\text{qflow}}$  described above, significant amounts of geomorphic change to the stream channel were observed at SBI over the course of the summer monsoon season (Figure 14). The stage data for SBI showed numerous instances of bed aggradation and degradation, which was not observed at MBI to the same degree. These differences may be because MBI did not experience enough moderate to high burn severity to promote widespread overland flow. Higher burn severity has been linked to increased runoff in several studies; high temperatures are necessary to generate the fine organic matter combustion that forms hydrophobic layers and modify the soil structure enough to reduce infiltration (Benavides-Solorio & MacDonald, 2005; Moody, 2005; Moody et al., 2008; Pierson et al., 2002). At MBI, 15% of watershed area was burned at moderate severity and none at high severity, compared to 39% moderate severity and 4% high severity at SBI.



**Figure 14.** Geomorphic change observed at SBI. After a large rainstorm on June 25, 2021, the stream sensor was covered with ~10cm of fine sediment. The debris marking the upper levels of the staff plate imply that a large amount of sediment was moved downstream. Photo courtesy of Stephanie Kampf.

For these reasons, the runoff response observed at SBI in the first year following the 2020 Cameron Peak fire is most comparable to the findings of other post-fire studies in this region. These studies often discuss the generation of infiltration excess overland flow in terms of the maximum 30- or 60- minute rainfall intensity needed to exceed the infiltration capacity of burned

soils and generate runoff. We report thresholds of  $MI_{60}$  values, which can be related to  $MI_{30}$  values from the literature using the equation:

$$MI_{60} = 0.57MI_{30} + 0.13$$

with all units in  $\text{mm hr}^{-1}$  (Wilson et al., 2018).

SBI had a  $MI_{60}$  threshold of  $4 \text{ mm hr}^{-1}$ , which agreed with other published threshold values. The high-confidence range for  $MI_{60}$  thresholds in  $1\text{-}15 \text{ km}^2$  watersheds was  $4\text{-}8 \text{ mm hr}^{-1}$  for the first 2 years following 3 Front Range wildfires: the 2000 Bobcat fire, the 2002 Hayman fire, and the 2012 High Park fire (Wilson et al., 2018). In years 1 and 2 after the 1996 Buffalo Creek fire,  $MI_{60}$  thresholds were  $3\text{-}5 \text{ mm hr}^{-1}$  in a  $27 \text{ km}^2$  basin (Moody, 2002). Reported thresholds were slightly higher ( $MI_{60} > 5 \text{ mm hr}^{-1}$ ) for the 2000 Cerro Grande fire in New Mexico (Moody et al., 2008). Different thresholds were reported for the immediate post-fire period following the 2010 Fourmile Canyon fire: a simulated infiltration study found that almost any intensity of rainstorm produced infiltration-excess runoff, while a watershed-scale study found that most responses were initiated when  $MI_{60}$  exceeded  $6 \text{ mm hr}^{-1}$  (Ebel, 2020; Murphy et al., 2015).

There has been limited prior research on the post-fire hydrologic impact in snowmelt-dominated environments. With these areas experiencing larger and more frequent fires, it is critical to understand if these regions carry the same risks of flooding and debris flows seen at lower elevations (Alizadeh et al., 2021; Higuera et al., 2021). The results of this study suggest that they do not; there is little evidence to suggest that the persistent snow sites generated infiltration excess overland flow to a significant degree. Although the burned PSZ sites had shorter lags to peak and duration of responses than their unburned counterpart, it did not approach the level of what we observed at SBI. Additionally, we observed no widespread

geomorphic channel change at the high elevation streams. These findings indicate that deep snowpack regions do not experience streamflow generation as a threshold behavior the same way that lower elevation sites have been observed to following a fire. All the  $MI_{60}$  thresholds in the PSZ were less than  $1 \text{ mm hr}^{-1}$ —low compared to the thresholds observed in the ISZ in this study and by past research in this region. As discussed above, however, this higher level of responsiveness is more easily attributable to deeper and longer lasting snowpack leading to high antecedent soil moisture during the summer months.

The differences in post-fire runoff generation between the two snow zones could be due to patterns of landscape features and surface roughness that affect overland flow and surface connectivity. For example, lower elevations of the Front Range have poorer soil development and more exposed bedrock compared to the high elevation areas (Rossi et al., 2020). These factors can work to rapidly concentrate overland flow in the ISZ. Surface flow in the PSZ might be further slowed due to a higher level of surface roughness. The dense, subalpine forests in this region accumulate higher levels of coarse ground litter than the sparse forests at lower elevations. Although the fire removed significant amounts of ground cover at all elevations, unburned or low burned patches of ground in the PSZ that intersected critical flow paths could have introduced roughness that slowed down overland flow (Liu et al., 2021).

Many high elevation areas in the Front Range are characterized by rolling topography, a landscape feature imparted by past glaciation. These local sinks and depressions, like those described above at MBP, disrupt overland flow by allowing water to pond and infiltrate before it can reach a stream channel. These patterns of surface connectivity can also influence the flow response by changing post-fire soil characteristics. It has been hypothesized that there exists a soil moisture threshold at which fire-induced water-repellent soils become hydrophilic again.

Following the 2000 Bobcat fire in the Front Range, a soil moisture content of 28% was found to reverse hydrophobicity in moderately burned soils (MacDonald & Huffman, 2004). The high soil moisture in the PSZ (Harrison et al. 2021) is more than sufficient to meet this threshold.

However, the Bobcat Fire study observed the 28% soil moisture threshold in a ponderosa and lodgepole pine forest in the ISZ; whether the same threshold applies in high elevation burned forests is unknown. MacDonald and Huffman (2004) also note that these thresholds can vary greatly based on soil type and texture, which was not accounted for in this study.

### **4.3. Limitations**

The goal of this analysis was to identify differences in the post-fire flow response between watersheds of varying burn severity across distinct elevation regions. There are several important limitations to consider when interpreting these results. First, the small sample size and short period of record introduce uncertainty as to whether the trends we identified hold true more generally. Second, post-fire streamflow generation is influenced by watershed attributes that can be highly variable. Spatial patterns of burn severity, soil type, ground cover, and surface sealing are important controls on post-fire streamflow generation when positioned along major flow paths, yet these factors were not well controlled between sites in this study (Benavides-Solorio & MacDonald, 2005; Moody et al., 2008, 2013; Saxe et al., 2018). Consequently, important factors that we did not consider may have influenced the observed flow responses. Third, data collection and manipulation added additional uncertainty to this analysis. Precipitation was measured with tipping bucket rain gages, which can underestimate rainfall due to site-specific characteristics like equipment tilt, canopy cover, and wind. Stage data recorded by stream pressure transducers had a noise range of ~1cm, making it difficult to accurately represent low flows and the start and end times of quickflow response intervals. The noise could have been lessened by using a

moving average or median filter, or summing the data hourly or daily; however, we chose to leave the data as is (on 15-minute intervals) to reflect the timing and magnitude of short-duration streamflow responses more accurately. Two burned sites experienced geomorphic channel change along the study reach, leading us to manually adjust the stage level in a way potentially not indicative of the true stream stage. Rating curves introduced further uncertainty in discharge, particularly during times of high flow. For example, the annual hydrographs for the intermittent sites showed that UI had higher peak flows than MBI and SBI (Figure 6). This higher peak could be due to UI receiving greater annual precipitation than the comparison watersheds in the intermittent zone (Harrison et al., 2021). Another explanation is that the stage-discharge equation for UI overestimates high flows, evidenced by the difference between the runoff ratio found by this study and that reported by Harrison et al. (2021). Though this may be the case, the results of the streamflow response analysis remain valid because the rating curve for UI performs well for the time range (June through October 2021) that was the focus of this study.

Finally, the method of digital hydrograph separation we used and the decision to uniformly dictate the quickflow hydrograph inflection point as the end of a QRI likely varied in effectiveness between watersheds. Other methods of determining the end of a flow response were considered, such as the first time step following event peak with quickflow at or below initial values, or when the rate of change reached some predetermined level. However, none of these methods worked as consistently well for all study sites—the inflection point was clearly identifiable for all the flow events analyzed, unlike the two characteristics described above. Additionally, hydrograph separation did not include attempts to adjust for the diurnal changes in streamflow. These may reflect near-surface groundwater activity or may be due to temperature sensitivity in the sensors. Most of the events were shorter than the diurnal cycles, so they were

not likely heavily influenced by these fluctuations; however, future analysis could address the diurnal signals in greater detail.

## 5. CONCLUSION

Rising temperatures and shifting fire regimes in the western United States are pushing fires upslope into areas of deep winter snowpack, necessitating a new understanding of how hydrologic processes in these areas change after a wildfire. To address this, we quantified differences in the timing and magnitude of streamflow response to summer rain events between watersheds of varying levels of burn severity and seasonal snowpack cover. Like previous studies, we found that catchments in the high-elevation persistent snow zone produced more total streamflow than those in the mid-elevation intermittent snow zone. PSZ streams were also more responsive to rainfall, responding to more than twice the amount of rain events than streams in the ISZ (56 compared to 25). This is likely due to wetter antecedent soil content at high elevations. The effect of burn severity on streamflow generation was more difficult to ascertain than the effect of elevation; site-specific differences appeared to exert an outsized influence on the magnitude of the flow response in both snow zones. One clear result related to flow magnitude, however, was the difference in summer low flows between the unburned and burned sites at all elevations: the burned streams had lower baseflows than their unburned counterparts.

The relationship between fire and the timing of flow production was clearer: higher burn severity was correlated with shorter times to peak flow and overall event duration. We observed this relationship in both snow zones; however, only the severely burned site in the ISZ showed evidence of widespread infiltration excess overland flow. The generation of flow at this site exhibited threshold behavior similar to that reported in other studies in the region—the  $MI_{60}$  threshold was  $4 \text{ mm hr}^{-1}$ . Differences in landscape features, increased surface roughness, and higher soil moisture content could explain why runoff was not generated in this way in the PSZ.

Future studies that examine the post-fire hydrology of a larger number of high-elevation watersheds for a longer time period are necessary to conclude whether these trends are representative across the Front Range, and more generally the western United States. At the same time, these results imply that high elevation burned areas may not be as much at risk for post-fire flooding and debris flows, and that expensive treatments that look to mitigate these hazards should be prioritized at more sensitive lower elevation regions.

## REFERENCES

- Addington, R. N., Aplet, G. H., Battaglia, M. A., Briggs, J. S., Brown, P. M., Cheng, A. S., ... & Wolk, B. (2018). Principles and practices for the restoration of ponderosa pine and dry mixed-conifer forests of the Colorado Front Range. RMRS-GTR-373. Fort Collins, CO: US Department of Agriculture, Forest Service, Rocky Mountain Research Station. 121 p., 373.
- Alizadeh, M. R., Abatzoglou, J. T., Luce, C. H., Adamowski, J. F., Farid, A., & Sadegh, M. (2021). Warming enabled upslope advance in western US forest fires. *Proceedings of the National Academy of Sciences*, 118(22), e2009717118.
- ARS (Agriculture Research Service ), 2013. Rainfall Intensity Summarization Tool (RIST) (Version 3.89) [computer software]. United States Department of Agriculture. Retrieved from <http://www.ars.usda.gov/Research/docs.htm?docid=3251>.
- BAER, “Cameron Peak Fire Forest Service Burned Area Emergency Response Executive Summary Arapaho Roosevelt National Forest December 15, 2020,” US Forest Service, 2020.
- Benavides-Solorio, J. de D., & MacDonald, L. H. (2005). Measurement and prediction of post-fire erosion at the hillslope scale, Colorado Front Range. *International Journal of Wildland Fire*, 14(4), 457. <https://doi.org/10.1071/WF05042>
- Blount, K., Ruybal, C. J., Franz, K. J., & Hogue, T. S. (2020). Increased water yield and altered water partitioning follow wildfire in a forested catchment in the western United States. *Ecohydrology*, 13(1). <https://doi.org/10.1002/eco.2170>
- Brown, T. C., Hobbins, M. T., & Ramirez, J. A. (2008). Spatial Distribution of Water Supply in the Conterminous United States 1. *JAWRA Journal of the American Water Resources Association*, 44(6), 1474–1487. <https://doi.org/10.1111/j.1752-1688.2008.00252>
- Calder, W. J., Parker, D., Stopka, C. J., Jiménez-Moreno, G., & Shuman, B. N. (2015). Medieval warming initiated exceptionally large wildfire outbreaks in the Rocky Mountains. *Proceedings of the National Academy of Sciences*, 112(43), 13261–13266. <https://doi.org/10.1073/pnas.1500796112>
- Cawson, J. G., Sheridan, G. J., Smith, H. G., & Lane, P. N. J. (2013). Effects of fire severity and burn patchiness on hillslope-scale surface runoff, erosion and hydrologic connectivity in a prescribed burn. *Forest Ecology and Management*, 310, 219–233. <https://doi.org/10.1016/j.foreco.2013.08.016>
- Clow, D. W. (2010). Changes in the timing of snowmelt and streamflow in Colorado: a response to recent warming. *Journal of Climate*, 23(9), 2293-2306.

- Day, T. J. (1976). On the precision of salt dilution gauging. *Journal of Hydrology*, 31(3-4), 293-306.
- Dunne, T., & Leopold, L. B. (1978). *Water in environmental planning*. Macmillan.
- Ebel, B. A. (2020). Temporal evolution of measured and simulated infiltration following wildfire in the Colorado Front Range, USA: Shifting thresholds of runoff generation and hydrologic hazards. *Journal of Hydrology*, 585, 124765. <https://doi.org/10.1016/j.jhydrol.2020.124765>
- Ebel, B. A., Moody, J. A., & Martin, D. A. (2012). Hydrologic conditions controlling runoff generation immediately after wildfire. *Water Resources Research*, 48(3).
- Emanuel, R. E., Hazen, A. G., McGlynn, B. L., & Jencso, K. G. (2014). Vegetation and topographic influences on the connectivity of shallow groundwater between hillslopes and streams. *Ecohydrology*, 7(2), 887-895.
- Fornwalt, P. J., Huckaby, L. S., Alton, S. K., Kaufmann, M. R., Brown, P. M., & Cheng, A. S. (2016). Did the 2002 Hayman Fire, Colorado, USA, Burn with Uncharacteristic Severity? *Fire Ecology*, 12(3), 117–132. <https://doi.org/10.4996/fireecology.1203117>
- Fritze, H., Stewart, I. T., & Pebesma, E. (2011). Shifts in western North American snowmelt runoff regimes for the recent warm decades. *Journal of Hydrometeorology*, 12(5), 989-1006.
- Fuka, D. R., Walter, M. T., Archibald, J. A., Steenhuis, T. S., Easton, Z. M., Fuka, M. D., & KeepSource, T. R. U. E. (2014). Package ‘EcoHydRology’.
- Gleeson, T., & Manning, A. H. (2008). Regional groundwater flow in mountainous terrain: Three-dimensional simulations of topographic and hydrogeologic controls. *Water Resources Research*, 44(10). <https://doi.org/10.1029/2008WR006848>
- Goeking, S. A., & Tarboton, D. G. (2020). Forests and Water Yield: A Synthesis of Disturbance Effects on Streamflow and Snowpack in Western Coniferous Forests. *Journal of Forestry*, 118(2), 172–192. <https://doi.org/10.1093/jofore/fvz069>
- Hallema, D. W., Moussa, R., Sun, G., & McNulty, S. G. (2016). Surface storm flow prediction on hillslopes based on topography and hydrologic connectivity. *Ecological Processes*, 5(1), 13. <https://doi.org/10.1186/s13717-016-0057-1>
- Hallema, D. W., Sun, G., Bladon, K. D., Norman, S. P., Caldwell, P. V., Liu, Y., & McNulty, S. G. (2017). Regional patterns of postwildfire streamflow response in the Western United States: The importance of scale-specific connectivity. *Hydrological Processes*, 31(14), 2582–2598. <https://doi.org/10.1002/hyp.11208>

- Hallema, D. W., Sun, G., Caldwell, P. V., Norman, S. P., Cohen, E. C., Liu, Y., Bladon, K. D., & McNulty, S. G. (2018). Burned forests impact water supplies. *Nature Communications*, 9(1), 1307. <https://doi.org/10.1038/s41467-018-03735-6>
- Hallema, D. W., Sun, G., Caldwell, P. V., Norman, S. P., Cohen, E. C., Liu, Y., Ward, E. J., & McNulty, S. G. (2017). Assessment of wildland fire impacts on watershed annual water yield: Analytical framework and case studies in the United States. *Ecohydrology*, 10(2), e1794. <https://doi.org/10.1002/eco.1794>
- Hammond, J. C., Saavedra, F. A., & Kampf, S. K. (2018). How does snow persistence relate to annual streamflow in mountain watersheds of the western US with wet maritime and dry continental climates?. *Water Resources Research*, 54(4), 2605-2623.
- Harpold, A. A., Molotch, N. P., Musselman, K. N., Bales, R. C., Kirchner, P. B., Litvak, M., & Brooks, P. D. (2015). Soil moisture response to snowmelt timing in mixed-conifer subalpine forests. *Hydrological Processes*, 29(12), 2782-2798.
- Harrison, H. N., Hammond, J. C., Kampf, S., & Kiewiet, L. (2021). On the hydrological difference between catchments above and below the intermittent-persistent snow transition. *Hydrological Processes*, 35(11). <https://doi.org/10.1002/hyp.14411>
- Higuera, P. E., Shuman, B. N., & Wolf, K. D. (2021). Rocky Mountain subalpine forests now burning more than any time in recent millennia. *Proceedings of the National Academy of Sciences*, 118(25), e2103135118. <https://doi.org/10.1073/pnas.2103135118>
- Hirsch, R. M., & De Cicco, L. (2015). User guide to Exploration and Graphics for RivEr Trends (EGRET) and dataRetrieval: R packages for hydrologic data, Techniques and Methods book 4, ch. A10. US Geological Survey, Reston, Virginia. <http://pubs.usgs.gov/tm/04/a10/>, accessed June.
- Kampf, S., Markus, J., Heath, J., & Moore, C. (2015). Snowmelt runoff and soil moisture dynamics on steep subalpine hillslopes. *Hydrological Processes*, 29(5), 712-723. <https://doi.org/10.1002/hyp.10179>
- Kampf, S. K., McGrath, D., Sears, M. G., Fassnacht, S. R., Kiewiet, L., & Hammond, J. C. (2022). Increasing wildfire impacts on snowpack in the western US. *Proceedings of the National Academy of Sciences*, 119(39), e2200333119.
- Kunze, M. D., & Stednick, J. D. (2006). Streamflow and suspended sediment yield following the 2000 Bobcat fire, Colorado. *Hydrological Processes*, 20(8), 1661-1681. <https://doi.org/10.1002/hyp.5954>
- Lenth, R., & Lenth, M. R. (2018). Package ‘lsmeans’. *The American Statistician*, 34(4), 216-221.

- Li, D., Wrzesien, M. L., Durand, M., Adam, J., & Lettenmaier, D. P. (2017). How much runoff originates as snow in the western United States, and how will that change in the future? *Geophysical Research Letters*, 44(12), 6163–6172. <https://doi.org/10.1002/2017GL073551>
- Liu, T., McGuire, L. A., Wei, H., Rengers, F. K., Gupta, H., Ji, L., & Goodrich, D. C. (2021). The timing and magnitude of changes to Hortonian overland flow at the watershed scale during the post-fire recovery process. *Hydrological Processes*, 35(5). <https://doi.org/10.1002/hyp.14208>
- Lyne, V., & Hollick, M. (1979, September). Stochastic time-variable rainfall-runoff modelling. In *Institute of Engineers Australia National Conference* (Vol. 79, No. 10, pp. 89-93). Barton, Australia: Institute of Engineers Australia.
- MacDonald, L. H., & Huffman, E. L. (2004). Post-fire Soil Water Repellency: Persistence and Soil Moisture Thresholds. *Soil Science Society of America Journal*, 68(5), 1729–1734. <https://doi.org/10.2136/sssaj2004.1729>
- Moody, J., 2002. An Analytical Method for Predicting Post-wildfire Peak Discharges. *U.S. Geological Survey Scientific Investigations Report 2011-5236*, 36 p
- Moody, J. A. (2005). Critical shear stress for erosion of cohesive soils subjected to temperatures typical of wildfires. *Journal of Geophysical Research*, 110(F1), F01004. <https://doi.org/10.1029/2004JF000141>
- Moody, J. A., & Martin, D. A. (2001). Initial hydrologic and geomorphic response following a wildfire in the Colorado Front Range. *Earth Surface Processes and Landforms*, 26(10), 1049–1070. <https://doi.org/10.1002/esp.253>
- Moody, J. A., Martin, D. A., Haire, S. L., & Kinner, D. A. (2008). Linking runoff response to burn severity after a wildfire. *Hydrological Processes*, 22(13), 2063–2074. <https://doi.org/10.1002/hyp.6806>
- Moody, J. A., Shakesby, R. A., Robichaud, P. R., Cannon, S. H., & Martin, D. A. (2013). Current research issues related to post-wildfire runoff and erosion processes. *Earth-Science Reviews*, 122, 10–37. <https://doi.org/10.1016/j.earscirev.2013.03.004>
- Moore, C., Kampf, S., Stone, B., & Richer, E. (2015). A GIS-based method for defining snow zones: Application to the western United States. *Geocarto International*, 30(1), 62–81. <https://doi.org/10.1080/10106049.2014.885089>
- Murphy, S. F., Writer, J. H., McCleskey, R. B., & Martin, D. A. (2015). The role of precipitation type, intensity, and spatial distribution in source water quality after wildfire. *Environmental Research Letters*, 10(8), 084007. <https://doi.org/10.1088/1748-9326/10/8/084007>

- Nathan, R. J., & McMahon, T. A. (1990). Evaluation of automated techniques for base flow and recession analyses. *Water resources research*, 26(7), 1465-1473.
- National Research Council. (2008). Hydrologic effects of a changing forest landscape. *National Academies Press*.
- Parks, S. A., Miller, C., Parisien, M.-A., Holsinger, L. M., Dobrowski, S. Z., & Abatzoglou, J. (2015). Wildland fire deficit and surplus in the western United States, 1984–2012. *Ecosphere*, 6(12), art275. <https://doi.org/10.1890/ES15-00294.1>
- Perry, T. D., & Jones, J. A. (2017). Summer streamflow deficits from regenerating Douglas fir forest in the Pacific Northwest, USA. *Ecohydrology*, 10(2), e1790.
- Pierson, F. B., Carlson, D. H., & Spaeth, K. E. (2002). Impacts of wildfire on soil hydrological properties of steep sagebrush-steppe rangeland. *International Journal of Wildland Fire*, 11(2), 145. <https://doi.org/10.1071/WF02037>
- Richer, E. E. (2009). Snowmelt runoff analysis and modeling for the Upper Cache la Poudre River Basin, Colorado (Doctoral dissertation, Colorado State University).
- Richer, E. E., Kampf, S. K., Fassnacht, S. R., & Moore, C. C. (2013). Spatiotemporal index for analyzing controls on snow climatology: Application in the Colorado Front Range. *Physical Geography*, 34(2), 85–107. <https://doi.org/10.1080/02723646.2013.787578>
- Rocca, M. E., Brown, P. M., MacDonald, L. H., & Carrico, C. M. (2014). Climate change impacts on fire regimes and key ecosystem services in Rocky Mountain forests. *Forest Ecology and Management*, 327, 290–305. <https://doi.org/10.1016/j.foreco.2014.04.005>
- Rossi, M. W., Anderson, R. S., Anderson, S. P., & Tucker, G. E. (2020). Orographic Controls on Subdaily Rainfall Statistics and Flood Frequency in the Colorado Front Range, USA. *Geophysical Research Letters*, 47(4). <https://doi.org/10.1029/2019GL085086>
- Saxe, S., Hogue, T. S., & Hay, L. (2018). Characterization and evaluation of controls on post-fire streamflow response across western US watersheds. *Hydrology and Earth System Sciences*, 22(2), 1221-1237.
- Schoener, G., & Stone, M. C. (2019). Impact of antecedent soil moisture on runoff from a semiarid catchment. *Journal of Hydrology*, 569, 627–636. <https://doi.org/10.1016/j.jhydrol.2018.12.025>
- Sidele, R. C., Tsuboyama, Y., Noguchi, S., Hosoda, I., Fujieda, M., & Shimizu, T. (1995). Seasonal hydrologic response at various spatial scales in a small forested catchment, Hitachi Ohta, Japan. *Journal of Hydrology*, 168(1–4), 227–250. [https://doi.org/10.1016/0022-1694\(94\)02639-S](https://doi.org/10.1016/0022-1694(94)02639-S)

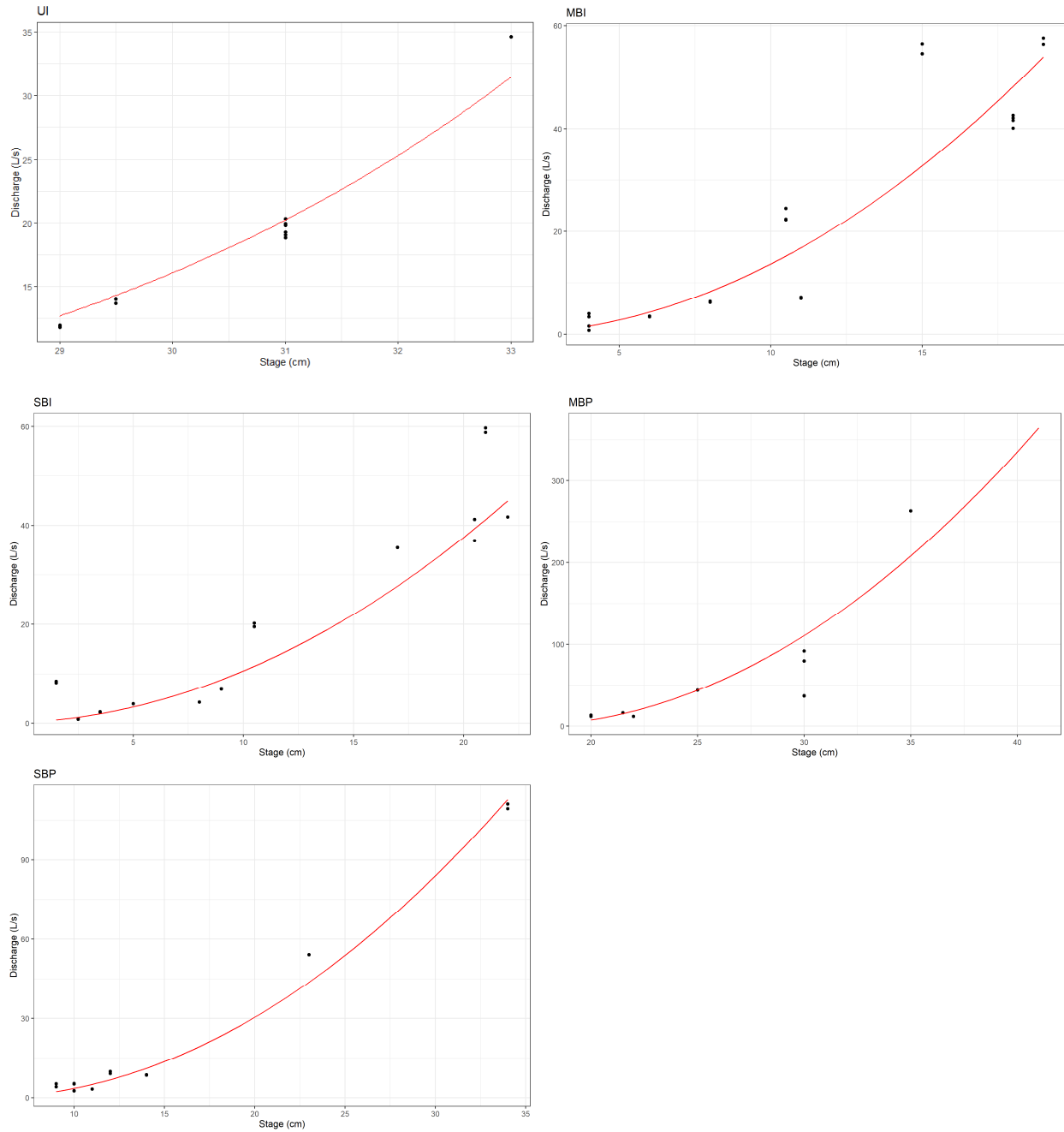
- Smith, R. S., Moore, R. D., Weiler, M., & Jost, G. (2014). Spatial controls on groundwater response dynamics in a snowmelt-dominated montane catchment. *Hydrology and Earth System Sciences*, 18(5), 1835–1856. <https://doi.org/10.5194/hess-18-1835-2014>
- Stewart, I. T., Cayan, D. R., & Dettinger, M. D. (2005). Changes toward earlier streamflow timing across western North America. *Journal of climate*, 18(8), 1136-1155.
- Viera, A. J., & Garrett, J. M. (2005). Understanding interobserver agreement: the kappa statistic. *Fam med*, 37(5), 360-363.
- Viviroli, D., Dürr, H. H., Messerli, B., Meybeck, M., & Weingartner, R. (2007). Mountains of the world, water towers for humanity: Typology, mapping, and global significance. *Water resources research*, 43(7).
- Westerling, A. L. (2016). Increasing western US forest wildfire activity: Sensitivity to changes in the timing of spring. *Philosophical Transactions of the Royal Society B: Biological Sciences*, 371(1696), 20150178. <https://doi.org/10.1098/rstb.2015.0178>
- Westerling, A. L., Hidalgo, H. G., Cayan, D. R., & Swetnam, T. W. (2006). Warming and Earlier Spring Increase Western U.S. Forest Wildfire Activity. *Science*, 313(5789), 940–943. <https://doi.org/10.1126/science.1128834>
- Westerling, A. L., Turner, M. G., Smithwick, E. A. H., Romme, W. H., & Ryan, M. G. (2011). Continued warming could transform Greater Yellowstone fire regimes by mid-21st century. *Proceedings of the National Academy of Sciences*, 108(32), 13165–13170. <https://doi.org/10.1073/pnas.1110199108>
- Wilson, C., Kampf, S. K., Wagenbrenner, J. W., & MacDonald, L. H. (2018). Rainfall thresholds for post-fire runoff and sediment delivery from plot to watershed scales. *Forest Ecology and Management*, 430, 346–356. <https://doi.org/10.1016/j.foreco.2018.08.025>
- U.S. Geological Survey. (2022). National water information system, USGS water data for the nation. Retrieved from <http://nwis.waterdata.usgs.gov/nwis>. Accessed February 1, 2022.
- Zambrano-Bigiarini, M. (2020). Package ‘hydroGOF’. Goodness-of-fit Functions for Comparison of Simulated and Observed.

## APPENDICES

Appendix A: Stage-discharge relationships

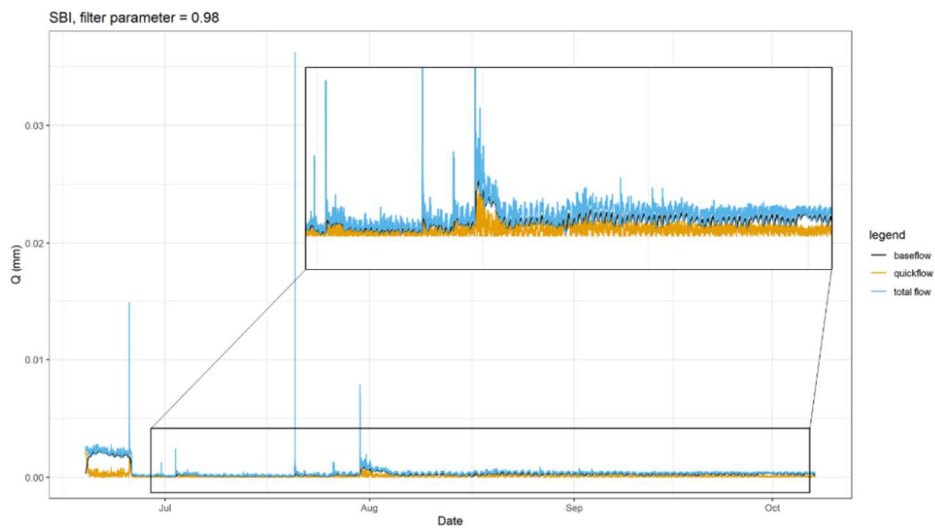
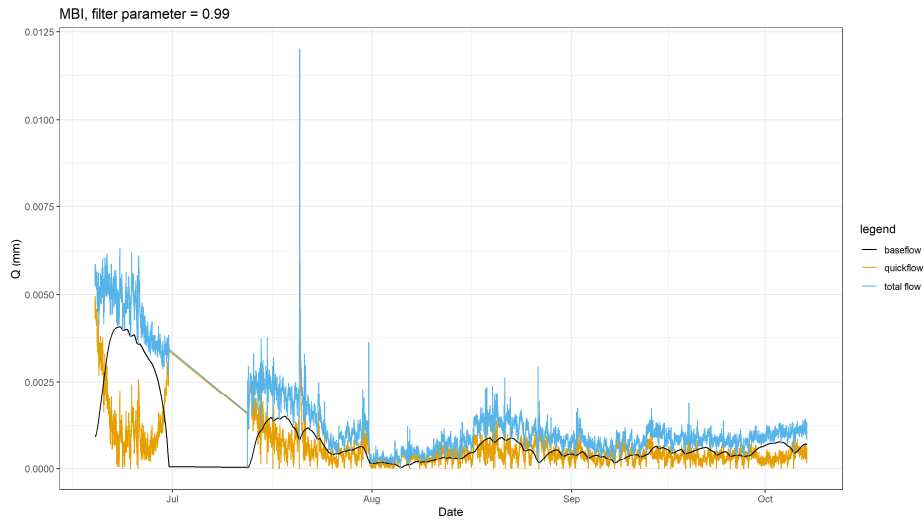
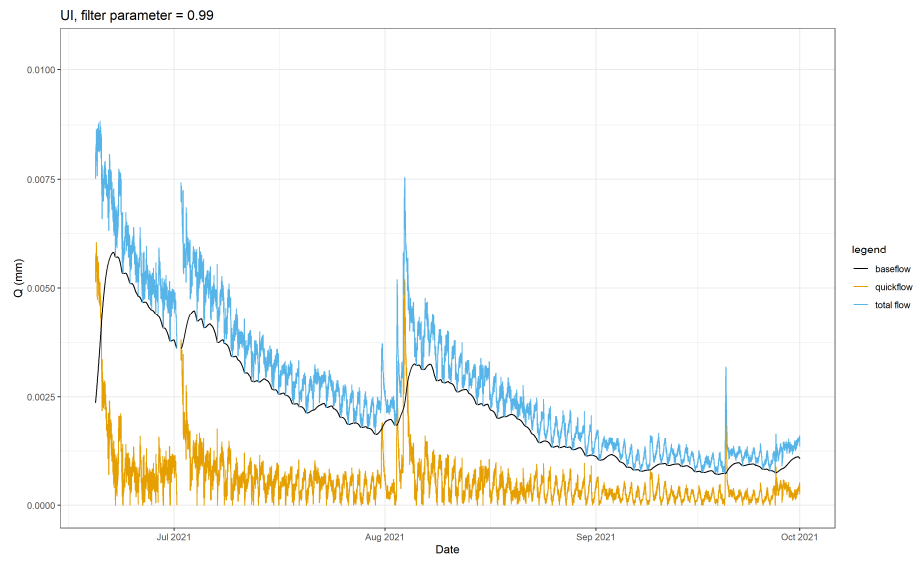
**Table A1.** Rating curve equations for stage-discharge for each study catchment. These equations estimate streamflow ( $y$ , L s<sup>-1</sup>) from stage height ( $h$ , cm).

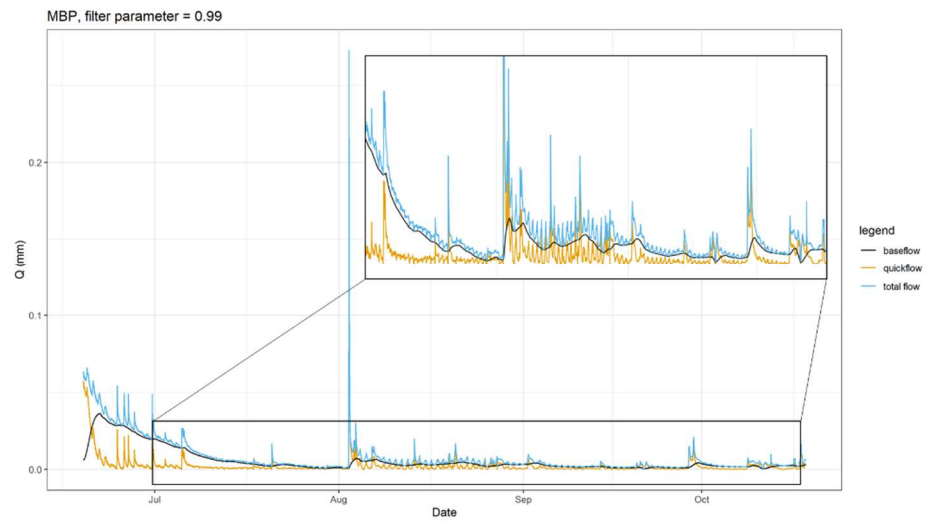
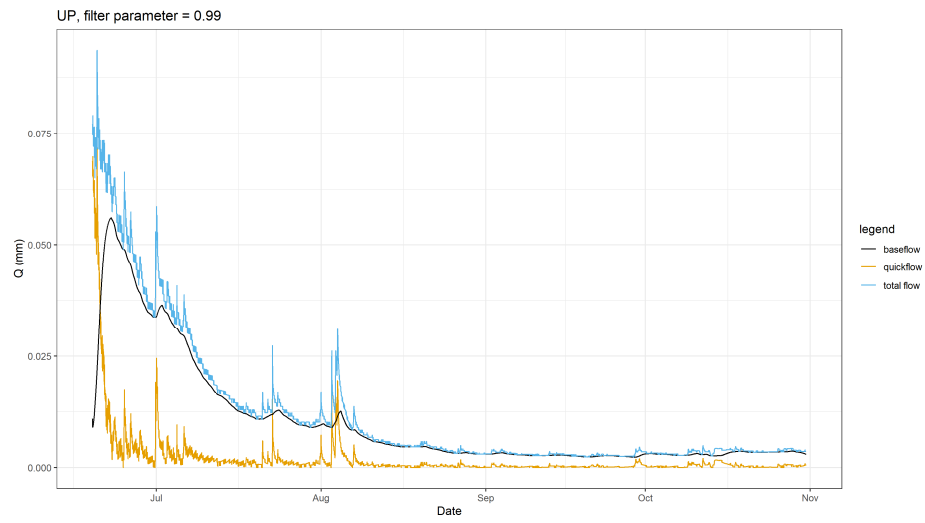
Site	Equation	R <sup>2</sup>
UI	$y=79505.577*\exp(-\exp(-0.0274184*(h-108.0802)))$	0.94
MBI	$y=(-0.353401+0.4052006*h)^2$	0.87
SBI	$y=(0.3764333+0.287650*h)^2$	0.93
UP	n/a	n/a
MBP	$y=(-12.8691+0.7795748*h)^2$	0.93
SBP	$y=(-1.776781+0.3647177*h)^2$	0.98



**Figure A1.** Relationship between manual discharge measurements ( $L s^{-1}$ ) and stream height (cm) for each study catchment.

## Appendix B: Digital baseflow separation for all study catchments





Appendix C: Table of Tukey's HSD p-values for comparisons between site and month.

Effect	Comparison	Model p-value				
		qflow	RR	T <sub>peak</sub>	D <sub>qflow</sub>	DR
site	UI-MBI	0.98	0.94	0.25	1.00	0.64
	UI-SBI	1.00	1.00	<b>0.00</b>	<b>0.00</b>	<b>0.00</b>
	UI-UP	<b>0.02</b>	<b>0.05</b>	<b>0.00</b>	1.00	0.99
	UI-MBP	<b>0.00</b>	<b>0.00</b>	1.00	0.98	1.00
	UI-SBP	<b>0.05</b>	0.08	1.00	1.00	0.89
	MBI-SBI	0.99	0.99	<b>0.01</b>	<b>0.00</b>	<b>0.01</b>
	MBI-UP	0.12	0.31	<b>0.00</b>	1.00	0.15
	MBI-MBP	<b>0.00</b>	<b>0.00</b>	<b>0.05</b>	0.93	0.72
	MBI-SBP	0.18	0.47	<b>0.05</b>	1.00	0.98
	SBI-UP	<b>0.04</b>	0.09	<b>0.00</b>	<b>0.00</b>	<b>0.00</b>
	SBI-MBP	<b>0.00</b>	<b>0.00</b>	<b>0.00</b>	<b>0.00</b>	<b>0.00</b>
	SBI-SBP	0.06	0.14	<b>0.00</b>	<b>0.00</b>	<b>0.00</b>
	UP-MBP	<b>0.01</b>	<b>0.04</b>	<b>0.00</b>	0.63	0.76
	UP-SBP	0.99	0.99	<b>0.00</b>	1.00	0.30
	MBP-SBP	<b>0.00</b>	<b>0.01</b>	1.00	0.90	0.95
month	6-7				0.99	0.48
	6-8				0.07	0.57
	6-9				<b>0.00</b>	<b>0.03</b>
	7-8				<b>0.02</b>	1.00
	7-9				<b>0.00</b>	0.37
	8-9				0.18	0.25

Appendix D: Coefficients for categorical variables used in streamflow response models.

**Table D1.** Coefficients for Site. Reference group is UI.

<b>y</b>	<b>MBI</b>	<b>SBI</b>	<b>UP</b>	<b>MBP</b>	<b>SBP</b>
<b>qflow</b>	0.29	0.10	1.16	2.01	1.01
<b>RR</b>	0.39	0.12	1.16	1.98	0.99
<b>T<sub>peak</sub></b>	-0.70	-1.79	1.16	0.04	0.04
<b>D<sub>qflow</sub></b>	0.05	-1.15	0.09	-0.14	0.01
<b>DR</b>	0.62	1.94	-0.20	0.16	0.38

**Table D2.** Coefficients for Month. Reference group is June.

<b>y</b>	<b>July</b>	<b>August</b>	<b>September</b>
<b>qflow</b>			
<b>RR</b>			
<b>T<sub>peak</sub></b>			
<b>D<sub>qflow</sub></b>	0.04	0.45	0.74
<b>DR</b>	-0.40	-0.35	-0.84